
1-Bit FQT: Pushing the Limit of Fully Quantized Training to 1-bit

Chang Gao

Beijing Jiaotong University
22110098@bjtu.edu.cn

Jianfei Chen

Tsinghua University
jianfeic@tsinghua.edu.cn

Kang Zhao

Tsinghua University
zhaokang29@huawei.com

Jiaqi Wang

Beijing Jiaotong University
jiaqi.wang@bjtu.edu.cn

Liping Jing

Beijing Jiaotong University
lpjing@bjtu.edu.cn

Abstract

Fully quantized training (FQT) accelerates the training of deep neural networks by quantizing the activations, weights, and gradients into lower precision. To explore the ultimate limit of FQT (the lowest achievable precision), we make a first attempt to 1-bit FQT. We provide a theoretical analysis of FQT based on Adam and SGD, revealing that the gradient variance influences the convergence of FQT. Building on these theoretical results, we introduce an Activation Gradient Pruning (AGP) strategy. The strategy leverages the heterogeneity of gradients by pruning less informative gradients and enhancing the numerical precision of remaining gradients to mitigate gradient variance. Additionally, we propose Sample Channel joint Quantization (SCQ), which utilizes different quantization strategies in the computation of weight gradients and activation gradients to ensure that the method is friendly to low-bitwidth hardware. Finally, we present a framework to deploy our algorithm. For fine-tuning VGGNet-16 and ResNet-18 on multiple datasets, our algorithm achieves an average accuracy improvement of approximately 6%, compared to per-sample quantization. Moreover, our training speedup can reach a maximum of 5.13× compared to full precision training. Ours code is available at <https://github.com/Gaochang-bjtu/1-bit-FQT>.

1 Introduction

Training neural networks has a high computational cost and memory footprint. Training with low-precision arithmetic (a.k.a., fully quantized training or FQT) can enhance computational and memory efficiency. FQT quantizes weights, activations, and gradients into low-bitwidth numerical formats, enabling a fast implementation of both forward and backward propagation on low-precision hardware.

The speedup potential of FQT depends on the numerical precision. Research aims to reduce the training numerical precision, without compromising convergence speed or accuracy. The required precision has been reduced from FP/INT16 Micikevicius et al. [2017], Das et al. [2018] to FP/INT8 Wang et al. [2018b], Banner et al. [2018], Zhu et al. [2020], Yang et al. [2020]. As of now, some work Sun et al. [2020], Chmiel et al. [2021], Xi et al. [2023] have successfully pushed precision down to 4 bits.

As the training numerical precision continues to decrease, a natural question arises:

What is the ultimate limit of FQT (i.e., the minimum achievable bitwidth)?

Answering this question not only advances our understanding of FQT but also provides a crucial direction for future hardware design strategies. Ideally, if we can push the bitwidth down to 1-bit, the training can be implemented with binary operations, such as XNOR and bitcounting operations Courbariaux et al. [2016], and hardware design might be greatly simplified. Binary computation is already shown possible for *inference* acceleration, such as XNOR-Net Rastegari et al. [2016], but 1-bit *training* remains unexplored.

Reducing the bitwidth for FQT is challenging because of (1) the lack of theoretical understanding, especially how gradient quantization affects the convergence; (2) the large quantization error of gradients, which causes a sharp performance drop or even divergence when reducing gradient bitwidth lower than 4-bit (Fig. 1). Due to these challenges, current research frontier is still 4-bit FQT.

In this work, we make a first attempt towards achieving 1-bit FQT. Firstly, we provide a theoretical analysis for FQT based on both Adam Kingma and Ba [2014] and SGD. Our analysis links the convergence with gradient variance. Specifically, our analysis reveals that Adam is more suitable for FQT than SGD in the low-bitwidth regime, due to their different sensitivity to gradient variance.

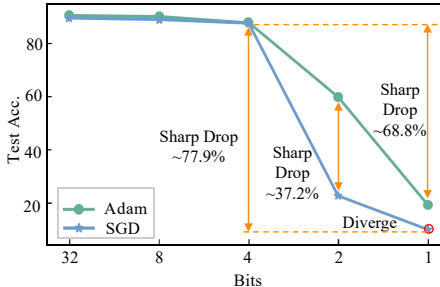


Figure 1: Gradient numerical precision (“bits”) vs. test accuracy of VGGNet16 on CIFAR-10, trained with Adam and SGD.

Inspired by the above theory, we propose a hardware-friendly algorithm for 1-bit FQT. Our algorithm consists of an Activation Gradient Pruning (AGP) method to reduce gradient variance, which is an improvement based on per-group quantizers Chen et al. [2020], Cho and Yoo [2020]. AGP utilizes gradient heterogeneity by discarding less informative groups, and allocate saved resources to improve the numerical precision of more informative ones. Additionally, we propose Sample Channel joint Quantization (SCQ), an effective quantization scheme for accelerated performance. SCQ employs different quantization methods for computing weight gradients and activation gradients, ensuring both can be effectively implemented on low bitwidth computing units.

We examine the potential of 1-bit FQT on transfer learning tasks in both vision and NLP domain. In this task, 1-bit FQT algorithm is used for on-device finetuning a pretrained 1-bit model to adapt new data. On all the datasets, our 1-bit FQT algorithm can successfully *converge* and demonstrate significantly superior performance compared to directly applying the previous FQT method to the task. The average accuracy drop on visual classification datasets is approximately 5%, compared to training the binary model with full-precision gradients. Notably, the average accuracy loss is negligible (less than 1%) on Flowers Nilsback and Zisserman [2008] dataset and Pets Parkhi et al. [2012] dataset, indicating that 1-bit FQT might indeed be useful in some cases. We implement our algorithm on Hygon and Raspberry Pi devices as a PyTorch-based library `binop`. Accelerated on-device training can be achieved with simple layer substitution, e.g., replace `torch.nn.Conv2d` with `binop.Conv2d`. In practice, our method can achieve up to 5.13× speedup, compared to FP32 PyTorch. These results indicate that in some specific tasks, FQT precision can be pushed to the ultimate 1-bit.

2 Related Works

Quantization Aware Training. QAT is a method designed to accelerate *inference* by quantizing the activations and weights. Various works Zhou et al. [2017], Choi et al. [2018], Zhang et al. [2018], Jacob et al. [2018], Dong et al. [2019], Tang et al. [2022], Liu et al. [2023] have been developed to quantize weights and activations into lower bitwidth. Furthermore, some studies Rastegari et al. [2016], Bulat and Tzimiropoulos [2019], Wang et al. [2020], Bai et al. [2020], Wu et al. [2023], Qin et al. [2023] have reduced the numerical precision of weights and activation values to 1 bit. However, QAT does not quantize gradients, and as a result, the backward propagation cannot be accelerated.

Fully Quantized Training. FQT further quantizes the gradients into lower precision, compared with QAT. Hence, FQT allows for efficient implementation of both forward and backward propagation on low-bitwidth computational units. FQT, unlike optimizer quantization Lin et al. [2022a], involves

quantizing weights, activations, and gradients altogether. Optimizer quantization only quantizes weight update (weight gradients), thus reducing communication costs but not accelerating computation Saha et al. [2022]. Early works on FQT use FP16 Gupta et al. [2015], Micikevicius et al. [2017] or INT16 Das et al. [2018] values to constrain weights, activations, and gradients. After that, various 8-bit numerical formats Wang et al. [2018b], Banner et al. [2018], Zhu et al. [2020], Yang et al. [2020], Xi et al. [2024] have been proposed that further push the bitwidth of data to 8 bits. Subsequently, Chen et al. [2020] provides theoretical bounds on how the quantization scheme (bitwidth, type of quantizer) affects the quality of the quantized gradient. Based on that, some works have successfully trained several networks with 4-bit activations/weights/gradients Sun et al. [2020], Chmiel et al. [2021], Xi et al. [2023]. The current research frontier is 4-bit FQT, but it still is not the ultimate limit.

3 Framework

To better describe our approach, necessary notations are introduced first. We denote the DNN model composed of L layers with the learnable parameter Θ as $\mathbf{F}(\cdot; \Theta)$. In each training iteration, we sample a minibatch (\mathbf{X}, \mathbf{Y}) from the dataset and input it into the model. The process is

$$\mathbf{H}^{(0)} = \mathbf{X}, \mathbf{H}^{(l)} = \mathbf{F}^{(l)}(\mathbf{H}^{(l-1)}; \Theta^{(l)}), \forall l \in [L]_+, \quad (1)$$

where $\mathbf{H}^{(l)} \in \mathbb{R}^{N \times D^{(l)}}$ is a feature map (N is the batch size, $D^{(l)}$ is the number of features), and $[L]_+ = \{1, 2, \dots, L\}$ are sets of integers. $\mathbf{F}^{(l)}$ is the l -th layer of the model with parameter $\Theta^{(l)}$. Given the minibatch loss $\mathcal{L}(\mathbf{H}^{(L)}, \mathbf{Y})$, we compute the gradient $\nabla_{\Theta^{(l)}} \mathcal{L}$, and update the parameter. For simplicity, we use $\nabla_{\mathbf{H}^{(l)}}$ and $\nabla_{\Theta^{(l)}}$ represent the activation/parameter gradient. The back-propagation is $\nabla_{\mathbf{H}^{(l-1)}}, \nabla_{\Theta^{(l)}} = \mathbf{B}^{(l)}(\nabla_{\mathbf{H}^{(l)}}, \mathbf{H}^{(l-1)}, \Theta^{(l)})$, where the function $\mathbf{B}^{(l)}(\cdot)$ takes the gradient of the output $\nabla_{\mathbf{H}^{(l)}}$ and the information kept in memory $(\mathbf{H}^{(l)}, \Theta^{(l)})$, and computes the gradient of the input. For example, consider a linear layer $\mathbf{H}^{(l)} = \mathbf{H}^{(l-1)} \Theta^{(l)}$ and its gradient is

$$\nabla_{\mathbf{H}^{(l-1)}} = \nabla_{\mathbf{H}^{(l)}} \Theta^{(l)\top}, \quad \nabla_{\Theta^{(l)}} = \mathbf{H}^{(l-1)\top} \nabla_{\mathbf{H}^{(l)}}. \quad (2)$$

3.1 Quantized Training

Here, we describe Quantization-Aware Training (QAT) and Fully Quantized Training (FQT). QAT is employed to accelerate *inference*, while FQT is designed to accelerate both *inference* and *training*.

Before embarking on QAT, the initial step involves quantizing the parameters and activations of the model: $\forall l \in [L]_+, \tilde{\mathbf{H}}^{(l-1)} = Q_f(\mathbf{H}^{(l-1)}), \tilde{\Theta}^{(l)} = Q_{\Theta}(\Theta^{(l)})$, where $Q_f(\cdot)$ and $Q_{\Theta}(\cdot)$ are quantizers for activations and weights, and $\tilde{\mathbf{H}}^{(l-1)}$ and $\tilde{\Theta}^{(l)}$ are quantized activations and weights. The forward propagation Eq. 1 is quantized as $\forall l \in [L]_+, \mathbf{H}^{(l)} = \mathbf{F}^{(l)}(\tilde{\mathbf{H}}^{(l-1)}; \tilde{\Theta}^{(l)})$, where $\tilde{\mathbf{H}}^{(l-1)}$ and $\tilde{\Theta}^{(l)}$ represent low-bit data. Therefore, the inference can be efficiently implemented on low-bitwidth computing kernels. QAT leverages the straight-through estimator Bengio et al. [2013] to train quantized models. The back-propagation Eq. 2 becomes: $\tilde{\nabla}_{\mathbf{H}^{(l-1)}} = \nabla_{\mathbf{H}^{(l)}} \tilde{\Theta}^{(l)\top}, \tilde{\nabla}_{\Theta^{(l)}} = \tilde{\mathbf{H}}^{(l-1)\top} \nabla_{\mathbf{H}^{(l)}}$. Since gradients are not quantized, the backpropagation cannot be accelerated.

The forward propagation of FQT is identical to QAT, FQT further quantizes the gradients at each layer as $\forall l \in [L]_+, \hat{\nabla}_{\mathbf{H}^{(l)}} = Q_g(\nabla_{\mathbf{H}^{(l)}})$, where $Q_g(\cdot)$ is a quantizer for gradients. The backpropagation is quantized as $\hat{\nabla}_{\mathbf{H}^{(l-1)}} = \hat{\nabla}_{\mathbf{H}^{(l)}} \tilde{\Theta}^{(l)\top}, \hat{\nabla}_{\Theta^{(l)}} = \tilde{\mathbf{H}}^{(l-1)\top} \hat{\nabla}_{\mathbf{H}^{(l)}}$, where $\hat{\nabla}_{\mathbf{H}^{(l)}}$ and $\hat{\nabla}_{\Theta^{(l)}}$ represent the FQT gradient. Now, with all operands quantized, the backpropagation can be efficiently implemented on low-bitwidth kernels.

3.2 FQT with Unbiased Quantizer

In our framework, $Q_f(\cdot)$ and $Q_{\Theta}(\cdot)$ are deterministic quantizers, while $Q_g(\cdot)$ is an unbiased quantizer. This configuration follows Chen et al. [2020]. In this framework, the gradients in FQT are unbiased estimates of QAT, ensuring both converge to the same point in expectation.

Consider Q_g as an unbiased stochastic quantizer, i.e., $\mathbb{E}[Q_g(\nabla_{\mathbf{H}})] = \nabla_{\mathbf{H}}$, for any $\nabla_{\mathbf{H}}$, which are already widely adopted in existing FQT approaches Banner et al. [2018], Xi et al. [2023], thereby

enabling $\mathbb{E}[\hat{\nabla}_{\mathbf{H}^{(l)}}] = \nabla_{\mathbf{H}^{(l)}}$. The activation gradients of FQT is $\mathbb{E}[\hat{\nabla}_{\mathbf{H}^{(l-1)}}] = \mathbb{E}[\hat{\nabla}_{\mathbf{H}^{(l)}}] \tilde{\Theta}^{(l)\top} = \tilde{\nabla}_{\mathbf{H}^{(l-1)}}$, which implies FQT and QAT convergence to a stationary point in expectation. Given an activation gradient tensor $\nabla_{\mathbf{H}}$, we quantize it to b -bit. We first compute the range of the tensor, and scale each element: $\bar{\nabla}_{\mathbf{H}_{i,j}} = \text{SR}(B(\nabla_{\mathbf{H}_{i,j}} - Z)/R)$, where $B = 2^b - 1$ are the number of quantization bins, $R = \max\{\nabla_{\mathbf{H}}\} - \min\{\nabla_{\mathbf{H}}\}$ is the range, $Z = \min\{\nabla_{\mathbf{H}}\}$ is the zero point, the stochastic rounding Courbariaux et al. [2015] operation $\text{SR}(\cdot)$ convert input to integers, and $\bar{\nabla}_{\mathbf{H}_{i,j}}$ is the gradient quantized to b bits. The dequantization is $\hat{\nabla}_{\mathbf{H}_{i,j}} = \bar{\nabla}_{\mathbf{H}_{i,j}} R/B + Z$. Due to the utilization of stochastic rounding, it is clear that $\mathbb{E}[\hat{\nabla}_{\mathbf{H}_{i,j}}] = \nabla_{\mathbf{H}_{i,j}}$.

The unbiased quantizer widely adopted in FQT is the per-group quantizer, including per-tensor quantizer (PTQ) Banner et al. [2018], per-sample quantizer (PSQ) Chen et al. [2020], and per-channel quantizer (PCQ) Cho and Yoo [2020]. In these strategies, each group computes its own range and zero point, rather than sharing a common one, which addresses the large variation of dynamic range across groups.

4 Theoretical Results

In this section, we analyze the convergence behavior of FQT under two different optimizers, Adam and SGD. The proof of theorems follows the framework in Kingma and Ba [2014], which can be found in Appendix A.

4.1 Optimizer Impact on Convergence

Quantized training with the Adam optimizer achieved much higher accuracy than those with SGD (Fig. 1). Although some prior studies Bulat and Tzimiropoulos [2019], Lin et al. [2022b] have highlighted this issue, the theoretical understanding of FQT with Adam is still lacking. To fill this gap, we will provide theoretical bounds on the convergence of FQT based on both Adam and SGD optimizers in the following part.

We use the framework proposed in Zinkevich [2003] to analyze the convergence. We adopt the assumption made by Zinkevich [2003] that the loss function \mathcal{L} is convex. At each iteration t , we predict using the parameter Θ_t and evaluate it on the loss function \mathcal{L}_t . We evaluate the convergence of FQT using the regret: $R(T) = \sum_{t=1}^T [\mathcal{L}_t(\Theta_t) - \mathcal{L}_t(\Theta^*)]$, where Θ^* are the best fixed point parameter. We define $\nabla_{\Theta_{1:t,i}} \in \mathbb{R}^t$ as a vector that contains the i -th dimension of the gradients over all iterations till t , $\nabla_{\Theta_{1:t,i}} = [\nabla_{\Theta_{1,i}}, \nabla_{\Theta_{2,i}}, \dots, \nabla_{\Theta_{t,i}}]$, $\hat{\nabla}_{\Theta_{1:t,i}}$ is the quantized version of $\nabla_{\Theta_{1:t,i}}$.

Assumption 4.1 *There exists $\sigma, e > 0$, such that $\forall \Theta_{t,i}$, $\text{Var}[\hat{\nabla}_{\Theta_{t,i}}] \leq \sigma^2$, $-e \leq \mathbb{E}[\hat{\nabla}_{\Theta_{t,i}}] \leq e$.*

Assumption 4.2 *The distance between any Θ_t is bounded, $\|\Theta_n - \Theta_m\|_2 \leq D$, $\|\Theta_n - \Theta_m\|_\infty \leq D_\infty$, for any $m, n \in \{1, \dots, T\}$.*

Given an unbiased gradient, we now establish the convergence of quantized training under SGD. The iteration form of SGD is $\Theta_{t+1} \leftarrow \Theta_t - \alpha_t \hat{\nabla}_{\Theta_t}$.

Theorem 4.3 *If Assumption 4.1 and 4.2 holds, let $\alpha_t = \frac{\alpha}{\sqrt{t}}$ and the number of elements in the gradient is d . SGD achieves the following guarantee, for all $T \geq 1$. $R^{SGD}(T) \leq \frac{D^2}{2\alpha} + \frac{\alpha T d(\sigma^2 + e^2)}{2}$.*

The iteration form of Adam is expressed as follows:

$$\begin{cases} m_t = \beta_{1,t} \cdot m_{t-1} + (1 - \beta_{1,t}) \cdot \hat{\nabla}_{\Theta_t}, v_t = \beta_2 \cdot v_{t-1} + (1 - \beta_2) \cdot \left(\hat{\nabla}_{\Theta_t}\right)^2, \\ \hat{m}_t = \frac{m_t}{1 - \beta_1^t}, \hat{v}_t = \frac{v_t}{1 - \beta_2^t}, \Theta_{t+1} = \Theta_t - \frac{\alpha}{\sqrt{\hat{v}_t + \epsilon}} \cdot \hat{m}_t. \end{cases}$$

Assumption 4.4 *The function \mathcal{L}_t has bounded gradients, $\forall \Theta$, $\|\hat{\nabla}_{\Theta_t}\|_2 \leq G$, $\|\hat{\nabla}_{\Theta_t}\|_\infty \leq G_\infty$.*

Theorem 4.5 *If Assumption 4.1, 4.2 and 4.4 holds, let $\beta_1, \beta_2 \in [0, 1)$ satisfy $\frac{\beta_1^2}{\sqrt{\beta_2}} < 1$, $\alpha_t = \frac{\alpha}{\sqrt{t}}$, and $\beta_{1,t} = \beta_1 \lambda^{t-1}$, $\lambda \in (0, 1)$. Adam achieves the following guarantee, for all $T \geq 1$.*

$$R^{Adam}(T) \leq \frac{((1-\lambda)^2 D^2 T + D_\infty^2) d}{2\alpha(1-\beta_1)(1-\lambda)^2} \sqrt{\sigma^2 + e^2} + \frac{\alpha(1+\beta_1)G_\infty \sqrt{T} d}{(1-\beta_1)\sqrt{1-\beta_2}(1-\gamma)^2} \sqrt{\sigma^2 + e^2}.$$

Based on Theorem 4.3, 4.5, Adam and SGD achieve the following guarantee, for $T \rightarrow \infty$. $\frac{R^{SGD}(T)}{T} \leq \alpha d(\sigma^2 + e^2)/2$, $\frac{R^{Adam}(T)}{T} \leq \frac{D^2 d}{2\alpha(1-\beta_1)} \sqrt{\sigma^2 + e^2}$. From the inqutation, it is straightforward to conclude that $\frac{R^{SGD}(T)}{T} = O(\sigma^2) + O(1)$, $\frac{R^{Adam}(T)}{T} = O(\sigma) + O(1)$. This implies that the convergence of FQT based on both Adam and SGD is influenced by the gradient variance, with SGD being more sensitive to variations in gradient variance.

4.2 Quantizer Impact on Gradient Variance

Based on our theory, gradient variance plays a crucial role in convergence. Gradient variance is primarily composed of two components: the variance of QAT gradients and the variance introduced by the gradient quantizers. Chen et al. [2020] reduced the complicated problem of gradient variance into the simple problem of quantizer variance. Thus, we need to minimize the quantizer variance.

The fundamental form of an unbiased quantizer Q_g is given by Sec. 3.2, and its variance is $\text{Var}[Q_g(\hat{\nabla}_{\mathbf{H}^{(l)}}) | \hat{\nabla}_{\mathbf{H}^{(l)}}] = \frac{R^2}{B^2} \text{Var}[\text{SR}(\cdot) | \hat{\nabla}_{\mathbf{H}^{(l)}}] \leq \frac{ND^{(l)}}{4B^2} R^2$, where the maximum variance of stochastic rounding $\text{SR}(\cdot)$ is 1/4. The expression reveals that as the bitwidth b decreases, the variance significantly increases. Furthermore, due to the sensitivity of SGD to gradient variance, SGD performs less effectively than Adam in low precision scenarios (large gradient variance) (Fig. 1). Therefore, in scenarios with larger gradient variances, such as in quantized training, the Adam optimizer is recommended. Additionally, the variance is highly sensitive to the gradient range R , with outliers in the gradient expanding the range and consequently increasing the quantizer’s variance.

5 1-bit FQT Algorithm

In this section, we propose our 1-bit FQT algorithm, including the quantization of weights, activation, and gradients.

5.1 Forward Propagation

In the forward propagation, both Q_f and Q_Θ are deterministic quantizers, taking the form: $\text{sign}(x) = -1$ if $x \leq 0$ otherwise 1. For a fully connected layer, the forward propagation is $\mathbf{H}^{(l)} = (\text{sign}(\mathbf{H}^{(l-1)}) \text{sign}(\Theta^{(l)})) \odot \Gamma$, where $\Gamma \in \mathbb{R}^{D^{(l)}}$ represents the shared scaling factor for both weights and activations, and it is learnable parameters. The form follows Bulat and Tzimiropoulos [2019].

5.2 Backward Propagation

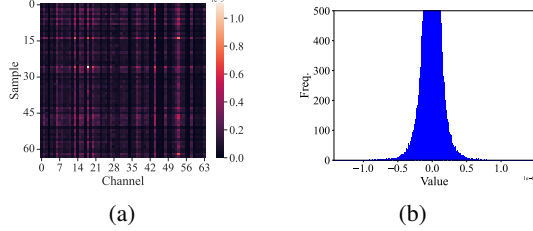
The form of backpropagation is

$$\hat{\nabla}_{\mathbf{H}^{(l-1)}} = Q_g(\hat{\nabla}_{\mathbf{H}^{(l)}}) \text{sign}(\Theta^{(l)\top}), \hat{\nabla}_{\Theta^{(l)}} = \text{sign}(\mathbf{H}^{(l-1)\top}) Q_g(\hat{\nabla}_{\mathbf{H}^{(l)}}). \quad (3)$$

Based on our theory, reducing quantizer variance is crucial to ensure the convergence of the model. However, outliers in the gradients can widen the range of gradients, thereby increasing variance.

To mitigate the impact of outliers on variance, per-group quantization is widely employed. Per-group quantization reduces variance by assigning a separate range to each group instead of sharing a large range among all. For example, we perform per-sample quantization on $\hat{\nabla}_{\mathbf{H}^{(l)}} \in \mathbb{R}^{N \times D^{(l)}}$ and its form is $Q_g(\hat{\nabla}_{\mathbf{H}_{i,j}^{(l)}}) = \text{SR}(B(\hat{\nabla}_{\mathbf{H}_{i,j}^{(l)}} - Z_i)/R_i)R_i/B + Z_i$, where R_i, Z_i represent the range and zero point of activation gradients for the i -th sample. Its variance is $\text{Var}[Q_g(\hat{\nabla}_{\mathbf{H}^{(l)}}) | \hat{\nabla}_{\mathbf{H}^{(l)}}] \leq \frac{D^{(l)}}{4B^2} \sum_{i=1}^N R_i^2$. However, the variance of PSQ is still too large for 1-bit FQT.

To address this, we propose Activation Gradient Pruning (AGP) to reduce quantizer variance. The gradients exhibit heterogeneity Xi et al. [2023], with some samples showing large gradient ranges, while the remaining gradients have smaller ranges. This pattern still holds true along the channel dimension, as illustrated in Fig. 2. Additionally, from the visualizations of gradient distributions, we observe that the elements in groups with smaller ranges are close to zero, indicating that less information stored in these groups. Therefore, we can prune groups with smaller ranges, reallocating the saved computational cost to groups with larger ranges, consequently enhancing the bitwidth of elements within those groups. Since variance mainly originates from groups with larger ranges, this approach effectively reduces variance.



Achieving 1-bit FQT based on the above idea requires ensuring three conditions: (1) if the bitwidth of retained groups is b , only $1/b$ of the groups can be preserved, thereby maintaining an average bitwidth of 1; (2) adopting random pruning to ensure the unbiased nature of quantization; (3) groups with larger ranges are more likely to be retained. Based on that, we first assign each group a probability $p_i \in [0, 1], i = 1, \dots, N$. To retain $\frac{N}{b}$ groups and ensure the retained groups have a large range, p_i needs to satisfy $\sum_{i=1}^N p_i = \frac{N}{b}$ and $p_i \propto R_i$, i.e., $p_i = \frac{NR_i}{bR_{total}}, R_{total} = \sum_{i=1}^N R_i$. Then we define random masks $m_i \sim \text{Bern}(p_i)$ to prune unimportant groups, and perform per-group quantization on the remaining ones. Its form is: $Q_g(\hat{\nabla}_{\mathbf{H}^{(l)}}) = Q_{PSQ}^b(\mathbf{M}\hat{\nabla}_{\mathbf{H}^{(l)}})$, where $\mathbf{M} = \text{diag}(\frac{m_1}{p_1}, \dots, \frac{m_N}{p_N})$, Q_{PSQ}^b is b -bit PSQ. Q_g is an unbiased quantizer since $\mathbb{E}[Q_{PSQ}^b(\mathbf{M}\hat{\nabla}_{\mathbf{H}^{(l)}})] = \mathbb{E}[\mathbf{M}]\hat{\nabla}_{\mathbf{H}^{(l)}} = \mathbf{I}\hat{\nabla}_{\mathbf{H}^{(l)}}$. The variance is

$$\text{Var} \left[Q_g \left(\hat{\nabla}_{\mathbf{H}^{(l)}} \right) \mid \hat{\nabla}_{\mathbf{H}^{(l)}} \right] \leq \frac{D^{(l)}}{4B^2} \sum_{i=1}^{\frac{N}{b}} R_i^2. \quad (4)$$

From Eq. 4, it can be observed that the variance of our quantizer is significantly smaller than that of 1-bit PSQ ($\frac{D^{(l)}}{4} \sum_{i=1}^N R_i^2$). The proof is given in Appendix B.

Despite reducing the average precision of each element to 1 bit through pruning, the practical acceleration is hindered by the fact that the retained groups maintain a precision of b -bit. We perform a lossless decomposition of the b -bit element: $x = \sum_{i=1}^b 2^{(i-1)}x^i$, where x^i represents the value at i -th bit of the b -bit element. Extend the decomposition operation to the entire tensor, Eq. 3 becomes: $\hat{\nabla}_{\mathbf{H}^{(l-1)}} = \sum_{i=1}^b 2^{(i-1)}(Q_g(\hat{\nabla}_{\mathbf{H}^{(l)}}))^i \text{sign}(\Theta^{(l)\top})$, $\hat{\nabla}_{\Theta^{(l)}} = \sum_{i=1}^b 2^{(i-1)}\text{sign}(\mathbf{H}^{(l-1)\top})(Q_g(\hat{\nabla}_{\mathbf{H}^{(l)}}))^i$, where $(Q_g(\hat{\nabla}_{\mathbf{H}^{(l)}}))^i$ represents the i -th binarized slice tensor of $Q_g(\hat{\nabla}_{\mathbf{H}^{(l)}})$, where each element represents the value at the i -th bit of the corresponding element in $Q_g(\hat{\nabla}_{\mathbf{H}^{(l)}})$. Due to the removal of some groups, the shape of the result differs from the original, and we fill the gaps with zeros. The entire process is illustrated in Fig. 3.

5.3 Practical Acceleration

In order to ensure the compatibility of our method with low-bit hardware, we first illustrate the necessary conditions for achieving practical acceleration through a PSQ example. The form of PSQ can be rewritten as: $Q_{PSQ}(\hat{\nabla}_{\mathbf{H}^{(l)}}) = \mathbf{S}_{float}\bar{\nabla}_{\mathbf{H}^{(l)}}$, where $\mathbf{S}_{float} = \text{diag}\{\frac{R_1}{B}, \dots, \frac{R_N}{B}\}$ is a FP32 tensor and $\bar{\nabla}_{\mathbf{H}^{(l)}}$ is a 1-bit tensor. The Eq. 3 can be rewritten as: $\hat{\nabla}_{\mathbf{H}^{(l-1)}} = \mathbf{S}_{float}\bar{\nabla}_{\mathbf{H}^{(l)}} \text{sign}(\Theta^{(l)\top})$, $\hat{\nabla}_{\Theta^{(l)}} = \text{sign}(\mathbf{H}^{(l-1)\top})\mathbf{S}_{float}\bar{\nabla}_{\mathbf{H}^{(l)}}$, where the computation of activation gradients $\hat{\nabla}_{\mathbf{H}^{(l-1)}}$ can be accelerated, as 1-bit matrix multiplication (MM) $\bar{\nabla}_{\mathbf{H}^{(l)}} \text{sign}(\Theta^{(l)\top})$ can be implemented efficiently on hardware. However, weight gradients $\hat{\nabla}_{\Theta^{(l)}}$ cannot be efficiently computed, as one of the two 1-bit tensors $\bar{\nabla}_{\mathbf{H}^{(l)}}$ needs to be dequantized to a full-precision tensor before their multiplication. This severely limits the acceleration.

To address this issue, we propose Sample Channel joint Quantization (SCQ), wherein PCQ is employed during the computation of weight gradients, while PSQ is utilized for the computation

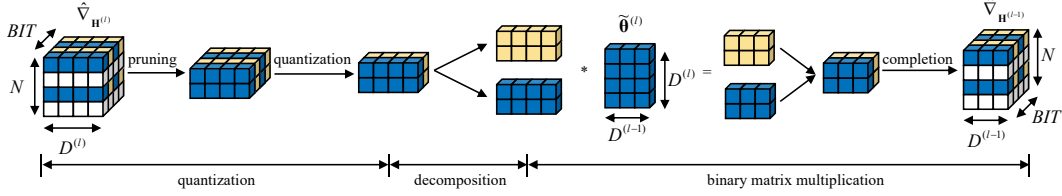


Figure 3: The process of AGP and binary matrix multiplication. BIT represents the bitwidth of full precision data. Here, we removed half of the groups, thus the bitwidth of the remaining groups is 2.

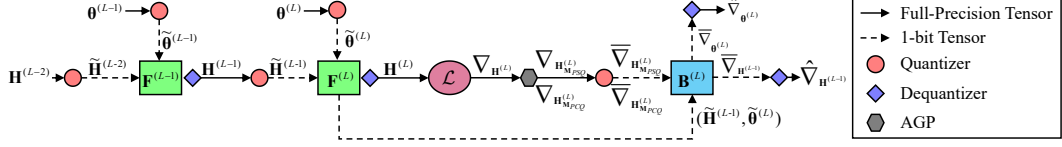


Figure 4: The computational graph of 1-bit FQT. The figure only shows the forward propagation of the last two layers and the backward propagation of the final layer.

of activation gradients. Building upon this quantization strategy, the backpropagation process can be rewritten as: $\hat{\nabla}_{\mathbf{H}^{(l-1)}} = \mathbf{S}_{PSQ} \bar{\nabla}_{\mathbf{H}_{PSQ}^{(l)}} \text{sign}(\Theta^{(l)\top})$, $\hat{\nabla}_{\Theta^{(l)}} = \text{sign}(\mathbf{H}^{(l-1)\top}) \bar{\nabla}_{\mathbf{H}_{PCQ}^{(l)}} \mathbf{S}_{PCQ}$, where $\mathbf{S}_{PCQ} = \text{diag} \left\{ \frac{R_1^c}{B}, \dots, \frac{R_{D^{(l)}}^c}{B} \right\}$, R_i^c represents the range of i -th channel. This strategy facilitates the acceleration of both weight and activation gradient computations. We integrate this strategy with the previously proposed AGP (Fig. 4), resulting in the final formulation: $\hat{\nabla}_{\mathbf{H}^{(l-1)}} = Q_{PSQ}^b \left(\mathbf{M}_{PSQ} \hat{\nabla}_{\mathbf{H}^{(l)}} \right) \text{sign}(\Theta^{(l)\top})$, $\hat{\nabla}_{\Theta^{(l)}} = \text{sign}(\mathbf{H}^{(l-1)\top}) Q_{PCQ}^b \left(\hat{\nabla}_{\mathbf{H}^{(l)}} \mathbf{M}_{PCQ} \right)$. Since PCQ treats a channel as a group, pruning operations also need to be performed along the channel dimension. Due to space constraints, decomposition and implementation details are provided in Appendix C.

6 Experiments

We evaluate our approach on transfer learning tasks. Although our approach is constrained to transfer learning, it still holds practical value in on-device training Lin et al. [2022b]. Due to challenges such as environmental constraints and limited memory, it is impractical to perform training from scratch on edge devices Ren et al. [2021]. The experiment details and results from training from scratch are in Appendix D.

6.1 Main Results

We employed two DNN architectures, ResNet18 He et al. [2016] and VGGNet16 Simonyan and Zisserman [2014]. We pre-trained them on ImageNet Deng et al. [2009] and subsequently conducted QAT. The quantized models are fine-tuned on downstream datasets to evaluate our approach. Following Lin et al. [2022b], we utilize various datasets, including Cars Krause et al. [2013], CIFAR-10 Krizhevsky et al. [2009], CIFAR-100 Krizhevsky et al. [2009], CUB Welinder et al. [2010], Flowers Nilsback and Zisserman [2008] and Pets Parkhi et al. [2012].

Converged model accuracy. To evaluate the performance of our method, we report the accuracy of two model architectures, VGG16 and ResNet18, across various datasets in Table 1. We report the mean and stddev of 3 runs. The compared approaches include QAT Bulat and Tzimiropoulos [2019] and PSQ. Since QAT employs training with full precision gradients, it can be considered as an upper bound for the accuracy of 1-bit FQT. Existing work has not tried 1-bit FQT, so we did not compare more methods. On VGGNet16, our method achieves $< 10\%$ average accuracy degradation across all configurations, as compared to the baseline QAT with 32-bit gradients. Moreover, in the optimal configuration ($b=4$), our method exhibit only approximately 5% average accuracy drop. On the more challenging ResNet18, the worst configuration ($b=2$) and the optimal configuration ($b=4$) achieves 9.47% and 5.57% average accuracy degradation, respectively, compared to QAT. Furthermore, on some datasets such as Flowers and Pets, our method exhibits minimal accuracy loss, indicating its suitability for these datasets. In summary, while our approach exhibits a notable decrease in accuracy compared to QAT, the incurred gap remains acceptable considering the benefits gained from reducing

Table 1: Experimental results on multiple downstream datasets. “(W, A, G)” denote the bitwidth of weight, activations, and gradients, respectively. b represents the bitwidth of the remaining groups.

Method	Precision (W, A, G)	Accuracy(%)						
		CIFAR-10	CIFAR-100	Flowers	Cars	Pets	CUB	Average
ResNet-18								
QAT	1, 1, 32	87.31±.25	65.82±.43	78.85±.80	50.81±.38	71.68±.21	42.13±.43	66.10
PSQ	8, 8, 8	92.90±.03	75.83±.05	85.96±.44	71.09±.71	87.86±.20	61.22±.05	79.14
PSQ	1, 1, 1	71.04±.61	47.71±.98	78.91±.10	23.14±.91	68.93±.39	34.29±.62	54.01
Ours ($b = 2$)	1, 1, 1	74.10±.21	52.19±.62	79.93±.20	26.51±.76	70.47±.52	36.59±.31	56.63
Ours ($b = 4$)	1, 1, 1	78.52±.56	56.83±.61	79.28±.50	37.88±.36	71.17±.16	39.47±.25	60.53
Ours ($b = 8$)	1, 1, 1	73.73±.99	52.64±.36	78.10±.65	29.78±.89	69.98±.32	37.01±.53	56.87
VGGNet-16								
QAT	1, 1, 32	89.80±.36	71.70±.17	86.86±.35	67.65±.03	79.49±.44	53.39±.57	74.82
PSQ	8, 8, 8	90.88±.07	73.12±.09	88.59±.15	81.27±.05	90.33±.03	69.49±.09	82.28
PSQ	1, 1, 1	80.60±.20	59.81±.20	84.65±.05	40.01±.88	77.20±.38	43.17±.44	64.24
Ours ($b = 2$)	1, 1, 1	82.66±.44	62.04±.01	85.75±.29	44.40±.92	77.77±.35	46.33±.53	66.49
Ours ($b = 4$)	1, 1, 1	84.38±.12	63.65±.19	87.12±.20	57.06±.60	78.48±.21	49.10±.17	69.97
Ours ($b = 8$)	1, 1, 1	78.14±.86	60.20±.08	86.24±.15	46.95±.21	77.39±.26	47.48±.20	66.07

Table 2: Comparison of training speedup across different input resolutions. "-Basic" and "Basic" represent unoptimized FQT and unoptimized FP32 training. The baseline is FP32 Pytorch.

Model	Method	Precision (W, A, G)	Hygon					Raspberry Pi 5		
			32	64	128	224	average	32	64	average
VGGNet-16	Basic	32, 32, 32	0.04×	0.03×	0.03×	0.02×	0.03×	0.05×	0.02×	0.04×
	PSQ-Basic	8, 8, 8	0.08×	0.06×	0.06×	0.06×	0.07×	0.10×	0.04×	0.07×
	SCQ-Basic	8, 8, 8	0.24×	0.18×	0.17×	0.15×	0.19×	0.23×	0.08×	0.16×
	Ours-Basic	1, 1, 1	4.36×	3.25×	3.19×	1.86×	3.17×	3.47×	1.17×	2.32×
	Ours	1, 1, 1	5.13×	3.71×	3.38×	2.73×	3.74×	3.72×	1.25×	2.49×
ResNet-18	Basic	32, 32, 32	0.03×	0.03×	0.03×	0.02×	0.03×	0.02×	0.02×	0.02×
	PSQ-Basic	8, 8, 8	0.07×	0.07×	0.06×	0.06×	0.07×	0.05×	0.03×	0.04×
	SCQ-Basic	8, 8, 8	0.17×	0.17×	0.16×	0.16×	0.17×	0.11×	0.08×	0.10×
	Ours-Basic	1, 1, 1	2.69×	2.75×	2.31×	1.30×	2.26×	1.33×	0.92×	1.13×
	Ours	1, 1, 1	2.93×	2.88×	2.62×	2.15×	2.65×	1.42×	0.97×	1.20×

the numerical precision of gradients to 1 bit. Additionally, we compared our method with 1-bit PSQ. Across both frameworks, our approach consistently outperformed it in terms of average accuracy across all configurations. Moreover, except for individual outcomes in the worst configuration, our method also exhibited superior accuracy across all datasets.

The value of b . We investigate the impact of hyperparameter b on performance and determine the optimal choice for b . From Eq. 4, as b increases, the variance of the quantizer gradually decreases, suggesting an improvement in training convergence. However, the increase in b also implies more discarded groups, leading to larger losses. Therefore, the choice of b becomes a trade-off issue. In Table 1, we report the accuracy of our method across various datasets under three different configurations ($b = 2$, $b = 4$, and $b = 8$). On VGGNet16 and ResNet18, the configuration with $b = 4$ consistently outperforms the others ($b = 2$ and $b = 8$) in terms of average accuracy. Moreover, this observation extends to the majority of datasets, where, even on a few datasets, the results for the configuration with $b = 4$ may not be optimal, the performance difference remains marginal compared to the optimal results. In conclusion, the optimal configuration is $b = 4$.

Effect of the optimizer. To validate our theory that the SGD optimizer is more sensitive to the variance of gradients compared to the Adam optimizer, we conduct a performance comparison of different optimizers on the CIFAR-10 dataset. We present the test accuracy curves of our method and PSQ across different optimizers in Fig. 5. For both methods, model performance degrades when using the SGD compared to the Adam. This is primarily attributed to the sensitivity of SGD to gradient variance. In addition, we observed that our method with SGD

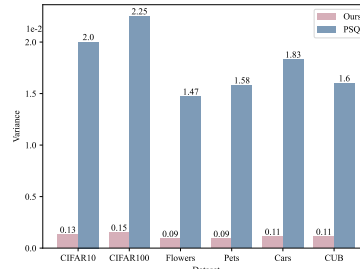


Figure 6: Quantizer variances across different datasets.

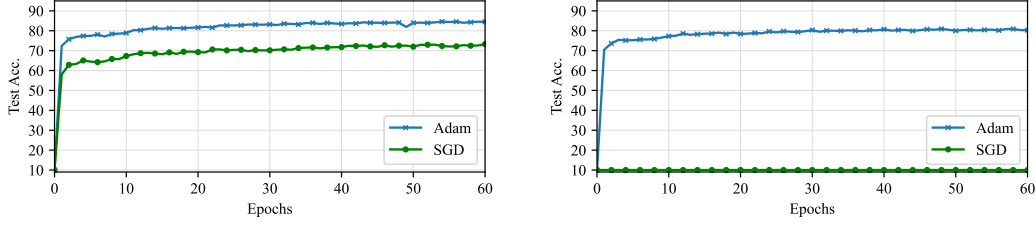


Figure 5: Our method (left) vs. PSQ (right): Testing accuracy on VGGNet16 for CIFAR-10.

experienced only a modest accuracy drop, whereas the PSQ method with SGD failed to converge entirely. We attribute this observation to the larger variance introduced by PSQ compared to our quantizer, resulting in divergence.

Variance. To demonstrate the advantages of our quantizer in reducing variance, we present the quantizer variance of ResNet18 in Fig. 6. In general, the quantizer variance of our method is lower than that of PSQ across all datasets. Additionally, the variance on the Flowers and Pets is lowest, explaining why the impact of quantization on accuracy is minor for them.

Other results. We report results for other architectures and tasks in Table 3. The details can be found in Appendix D. On Faster R-CNN Ren et al. [2015], our approach with 1-bit gradients achieves 1.66% mAP degradation, as compared to the baseline QAT with 32-bit gradients. In addition, for Mixer-MLP Tolstikhin et al. [2021], an all-MLP architecture, our approach shows a decrease of 3.52% in classification accuracy compared to the baseline. For BERT, our approach achieves 8.39% average performance degradation. These results indicate the potential of our approach to transfer to other architectures and tasks.

6.2 Computational Efficiency

We discuss the computational overhead of our method. Our implementation is not fully optimized, as the comprehensive hardware-algorithm co-design is beyond the scope of this paper. Our experiments are conducted on a single-core Hygon CPU and edge device (Raspberry Pi 5).

Training speedup. We compare the training time of the FP32 PyTorch and our 1-bit FQT for VGGNet16 and ResNet18. We vary the resolution of the input and summarize the speedup of our method in Table 2. For VGGNet16, our algorithm achieves an average speedup of 3.74 \times and 2.49 \times on the Hygon and edge device, respectively. For ResNet18, our algorithm achieves 2.65 \times and 1.20 \times average speedup. Additionally, to assess the acceleration potential of 1-bit FQT, we compare their speedup under the condition without optimization (Ours-Basic and Basic). The results indicate that across multiple cases, the speedup is well above a *hundredfold*. On edge devices, our method achieves a speedup of over 50 \times . This gap indicates significant acceleration potential for 1-bit FQT. Finally, we compare the speedup across layers of VGGNet16 and the time consumption for each operation in Appendix D, providing guidance for future optimization directions.

8-bit PSQ vs. Ours. To demonstrate the advantages of our method over other high-bit-width FQT methods, we compare our approach with 8-bit PSQ in terms of both speedup and classification performance (there is no 4-bit format among the standard data types). Table 1 reveals that compared to 8-bit PSQ, our method experiences an average accuracy reduction of 18.61% and 12.31% on ResNet18 and VGG16, respectively. Despite significant performance degradation, our approach achieves an average speedup of 32.28 \times and 45.28 \times over 8-bit PSQ on ResNet18 and VGG16, respectively. On Raspberry Pi 5, our speedup can also reach approximately 30 \times . Even when compared to hardware-friendly SCQ, 1-bit FQT achieves a speedup of over 10 \times (Table 2) Therefore, our method can be particularly beneficial in scenarios sensitive to time overhead.

Average 1-bit vs. 1-bit. We compared the runtime of average 1-bit matrix multiplication and 1-bit matrix multiplication across different matrix sizes in Table 4. The results demonstrate that the difference in runtime between these two methods is minimal, indicating similarity in the runtime of our average 1-bit FQT and 1-bit FQT. The analysis is provided in the Appendix C.

Table 3: Object detection on PASCAL VOC, classification on CIFAR-100 and NLP tasks on GLUE.

Task	Model	Method	Bits	mAP/Acc./Avg.
Det.	Faster R-CNN	QAT	32	52.34
	Faster R-CNN	Ours	1	50.68
Cls.	MLP-Mixer	QAT	32	52.17
	MLP-Mixer	Ours	1	48.65
NLP	BERT	QAT	32	63.20
	BERT	Ours	1	54.81

Table 4: Average 1-bit vs. 1-bit. The running time of matrix multiplication involving various sizes.

Setting	Time(ms) across various sizes					
	512	512	1024	1024	2048	2048
	512	1024	512	1024	512	1024
Average 1-bit	8.40	15.92	16.61	31.03	32.22	61.33
1-bit	8.01	14.54	15.91	29.79	29.92	59.94

7 Conclusion

We propose a hardware-friendly 1-bit FQT method in this work, which pushes the limit of FQT. Through convergence analysis, we propose AGP to reduce the variance of the quantizer, thereby enhancing the convergence of quantized training. Subsequently, to address the issue of unacceleratable weight gradient computation, we present a SCQ strategy. Finally, we propose a framework that practically accelerates training, achieving a speedup of up to 5.13 \times compared to full precision training. While our approach focuses solely on convolutional neural networks in this study, experiments indicate its potential applicability to other architectures.

Limitations: The primary limitation of this work lies in its ability to achieve 1-bit FQT in transfer learning tasks but not in training from scratch. To the best of our knowledge, even the 3-bit FQT from scratch is still an open problem.

Broader Impact

The introduction of 1-bit Fully Quantized Training (FQT) presents a significant advancement in deep neural network training, promising accelerated model training. Recently, huge models Brown et al. [2020] have achieved remarkable results across various domains. However, the training cost of these models is becoming increasingly expensive. The escalating training costs are leading to a growing dependence on computational resources in machine learning research, which raises concerns about fairness. FQT can effectively reduce the training expenses, thereby democratizing model training for a broader audience. Additionally, 1-bit FQT makes training on edge devices feasible. The models deployed on edge devices require updates when learning new data. However, due to environmental and memory constraints, these models cannot be directly updated Ren et al. [2021]. One straightforward approach is to conduct training directly on the edge device. However, the computational resources of edge devices are often insufficient to support model training. 1-bit FQT holds the promise of addressing this challenge.

References

- Haoli Bai, Wei Zhang, Lu Hou, Lifeng Shang, Jing Jin, Xin Jiang, Qun Liu, Michael Lyu, and Irwin King. Binarybert: Pushing the limit of bert quantization. *arXiv preprint arXiv:2012.15701*, 2020.
- Ron Banner, Itay Hubara, Elad Hoffer, and Daniel Soudry. Scalable methods for 8-bit training of neural networks. *Advances in neural information processing systems*, 31, 2018.
- Yoshua Bengio, Nicholas Léonard, and Aaron Courville. Estimating or propagating gradients through stochastic neurons for conditional computation. *arXiv preprint arXiv:1308.3432*, 2013.
- Tom Brown, Benjamin Mann, Nick Ryder, Melanie Subbiah, Jared D Kaplan, Prafulla Dhariwal, Arvind Neelakantan, Pranav Shyam, Girish Sastry, Amanda Askell, et al. Language models are few-shot learners. *Advances in neural information processing systems*, 33:1877–1901, 2020.
- Adrian Bulat and Georgios Tzimiropoulos. Xnor-net++: Improved binary neural networks. *arXiv preprint arXiv:1909.13863*, 2019.
- Jianfei Chen, Yu Gai, Zhewei Yao, Michael W Mahoney, and Joseph E Gonzalez. A statistical framework for low-bitwidth training of deep neural networks. *Advances in neural information processing systems*, 33: 883–894, 2020.

- Brian Chmiel, Ron Banner, Elad Hoffer, Hilla Ben Yaacov, and Daniel Soudry. Logarithmic unbiased quantization: Practical 4-bit training in deep learning. 2021.
- Seunghwan Cho and Sungjoo Yoo. Per-channel quantization level allocation for quantizing convolutional neural networks. In *2020 IEEE International Conference on Consumer Electronics-Asia (ICCE-Asia)*, pages 1–3. IEEE, 2020.
- Jungwook Choi, Zhuo Wang, Swagath Venkataramani, Pierce I-Jen Chuang, Vijayalakshmi Srinivasan, and Kailash Gopalakrishnan. Pact: Parameterized clipping activation for quantized neural networks. *arXiv preprint arXiv:1805.06085*, 2018.
- Mathieu Courbariaux, Yoshua Bengio, and Jean-Pierre David. Binaryconnect: Training deep neural networks with binary weights during propagations. *Advances in neural information processing systems*, 28, 2015.
- Mathieu Courbariaux, Itay Hubara, Daniel Soudry, Ran El-Yaniv, and Yoshua Bengio. Binarized neural networks: Training deep neural networks with weights and activations constrained to+ 1 or-1. *arXiv preprint arXiv:1602.02830*, 2016.
- Dipankar Das, Naveen Mellempudi, Dheevatsa Mudigere, Dhiraj Kalamkar, Sasikanth Avancha, Kunal Banerjee, Srinivas Sridharan, Karthik Vaidyanathan, Bharat Kaul, Evangelos Georganas, et al. Mixed precision training of convolutional neural networks using integer operations. *arXiv preprint arXiv:1802.00930*, 2018.
- Jia Deng, Wei Dong, Richard Socher, Li-Jia Li, Kai Li, and Li Fei-Fei. Imagenet: A large-scale hierarchical image database. In *2009 IEEE conference on computer vision and pattern recognition*, pages 248–255. Ieee, 2009.
- Zhen Dong, Zhewei Yao, Amir Gholami, Michael W Mahoney, and Kurt Keutzer. Hawq: Hessian aware quantization of neural networks with mixed-precision. In *Proceedings of the IEEE/CVF International Conference on Computer Vision*, pages 293–302, 2019.
- Suyog Gupta, Ankur Agrawal, Kailash Gopalakrishnan, and Pritish Narayanan. Deep learning with limited numerical precision. In *International conference on machine learning*, pages 1737–1746. PMLR, 2015.
- Kaiming He, Xiangyu Zhang, Shaoqing Ren, and Jian Sun. Deep residual learning for image recognition. In *Proceedings of the IEEE conference on computer vision and pattern recognition*, pages 770–778, 2016.
- Benoit Jacob, Skirmantas Kligys, Bo Chen, Menglong Zhu, Matthew Tang, Andrew Howard, Hartwig Adam, and Dmitry Kalenichenko. Quantization and training of neural networks for efficient integer-arithmetic-only inference. In *Proceedings of the IEEE conference on computer vision and pattern recognition*, pages 2704–2713, 2018.
- Diederik P Kingma and Jimmy Ba. Adam: A method for stochastic optimization. *arXiv preprint arXiv:1412.6980*, 2014.
- Jonathan Krause, Michael Stark, Jia Deng, and Li Fei-Fei. 3d object representations for fine-grained categorization. In *Proceedings of the IEEE international conference on computer vision workshops*, pages 554–561, 2013.
- Alex Krizhevsky, Geoffrey Hinton, et al. Learning multiple layers of features from tiny images. 2009.
- Chung-Yi Lin, Victoria Kostina, and Babak Hassibi. Differentially quantized gradient methods. *IEEE Transactions on Information Theory*, 68(9):6078–6097, 2022a.
- Ji Lin, Ligeng Zhu, Wei-Ming Chen, Wei-Chen Wang, Chuang Gan, and Song Han. On-device training under 256kb memory. *Advances in Neural Information Processing Systems*, 35:22941–22954, 2022b.
- Zechun Liu, Barlas Oguz, Changsheng Zhao, Ernie Chang, Pierre Stock, Yashar Mehdad, Yangyang Shi, Raghuraman Krishnamoorthi, and Vikas Chandra. Llm-qat: Data-free quantization aware training for large language models. *arXiv preprint arXiv:2305.17888*, 2023.
- Paulius Micikevicius, Sharan Narang, Jonah Alben, Gregory Diamos, Erich Elsen, David Garcia, Boris Ginsburg, Michael Houston, Oleksii Kuchaiev, Ganesh Venkatesh, et al. Mixed precision training. *arXiv preprint arXiv:1710.03740*, 2017.
- Maria-Elena Nilsback and Andrew Zisserman. Automated flower classification over a large number of classes. In *2008 Sixth Indian conference on computer vision, graphics & image processing*, pages 722–729. IEEE, 2008.

- Omkar M Parkhi, Andrea Vedaldi, Andrew Zisserman, and CV Jawahar. Cats and dogs. In *2012 IEEE conference on computer vision and pattern recognition*, pages 3498–3505. IEEE, 2012.
- Haotong Qin, Yifu Ding, Mingyuan Zhang, Qinghua Yan, Aishan Liu, Qingqing Dang, Ziwei Liu, and Xianglong Liu. Bibert: Accurate fully binarized bert. *arXiv preprint arXiv:2203.06390*, 2022.
- Haotong Qin, Xiangguo Zhang, Ruihao Gong, Yifu Ding, Yi Xu, and Xianglong Liu. Distribution-sensitive information retention for accurate binary neural network. *International Journal of Computer Vision*, 131(1): 26–47, 2023.
- Mohammad Rastegari, Vicente Ordonez, Joseph Redmon, and Ali Farhadi. Xnor-net: Imagenet classification using binary convolutional neural networks. In *European conference on computer vision*, pages 525–542. Springer, 2016.
- Haoyu Ren, Darko Anicic, and Thomas A Runkler. Tinyol: Tinymml with online-learning on microcontrollers. In *2021 International Joint Conference on Neural Networks (IJCNN)*, pages 1–8. IEEE, 2021.
- Shaoqing Ren, Kaiming He, Ross Girshick, and Jian Sun. Faster r-cnn: Towards real-time object detection with region proposal networks. *Advances in neural information processing systems*, 28, 2015.
- Rajarshi Saha, Mert Pilanci, and Andrea J Goldsmith. Efficient randomized subspace embeddings for distributed optimization under a communication budget. *IEEE Journal on Selected Areas in Information Theory*, 3(2): 183–196, 2022.
- Karen Simonyan and Andrew Zisserman. Very deep convolutional networks for large-scale image recognition. *arXiv preprint arXiv:1409.1556*, 2014.
- Xiao Sun, Naigang Wang, Chia-Yu Chen, Jiamin Ni, Ankur Agrawal, Xiaodong Cui, Swagath Venkataramani, Kaoutar El Maghraoui, Vijayalakshmi Viji Srinivasan, and Kailash Gopalakrishnan. Ultra-low precision 4-bit training of deep neural networks. *Advances in Neural Information Processing Systems*, 33:1796–1807, 2020.
- Hanlin Tang, Xipeng Zhang, Kai Liu, Jianchen Zhu, and Zhanhui Kang. Mq-bert: Quantized bert with 4-bits weights and activations. *arXiv preprint arXiv:2203.13483*, 2022.
- Ilya O Tolstikhin, Neil Houlsby, Alexander Kolesnikov, Lucas Beyer, Xiaohua Zhai, Thomas Unterthiner, Jessica Yung, Andreas Steiner, Daniel Keysers, Jakob Uszkoreit, et al. Mlp-mixer: An all-mlp architecture for vision. *Advances in neural information processing systems*, 34:24261–24272, 2021.
- Alex Wang, Amanpreet Singh, Julian Michael, Felix Hill, Omer Levy, and Samuel R Bowman. Glue: A multi-task benchmark and analysis platform for natural language understanding. *arXiv preprint arXiv:1804.07461*, 2018a.
- Naigang Wang, Jungwook Choi, Daniel Brand, Chia-Yu Chen, and Kailash Gopalakrishnan. Training deep neural networks with 8-bit floating point numbers. *Advances in neural information processing systems*, 31, 2018b.
- Ziwei Wang, Ziyi Wu, Jiwen Lu, and Jie Zhou. Bidet: An efficient binarized object detector. In *Proceedings of the IEEE/CVF conference on computer vision and pattern recognition*, pages 2049–2058, 2020.
- Peter Welinder, Steve Branson, Takeshi Mita, Catherine Wah, Florian Schroff, Serge Belongie, and Pietro Perona. Caltech-ucsd birds 200. 2010.
- Xiao-Ming Wu, Dian Zheng, Zuhao Liu, and Wei-Shi Zheng. Estimator meets equilibrium perspective: A rectified straight through estimator for binary neural networks training. In *Proceedings of the IEEE/CVF International Conference on Computer Vision*, pages 17055–17064, 2023.
- Haocheng Xi, Changhao Li, Jianfei Chen, and Jun Zhu. Training transformers with 4-bit integers. *arXiv preprint arXiv:2306.11987*, 2023.
- Haocheng Xi, Yuxiang Chen, Kang Zhao, Kaijun Zheng, Jianfei Chen, and Jun Zhu. Jetfire: Efficient and accurate transformer pretraining with int8 data flow and per-block quantization. *arXiv preprint arXiv:2403.12422*, 2024.
- Yukuan Yang, Lei Deng, Shuang Wu, Tianyi Yan, Yuan Xie, and Guoqi Li. Training high-performance and large-scale deep neural networks with full 8-bit integers. *Neural Networks*, 125:70–82, 2020.
- Dongqing Zhang, Jiaolong Yang, Dongqiangzi Ye, and Gang Hua. Lq-nets: Learned quantization for highly accurate and compact deep neural networks. In *Proceedings of the European conference on computer vision (ECCV)*, pages 365–382, 2018.

- Aojun Zhou, Anbang Yao, Yiwen Guo, Lin Xu, and Yurong Chen. Incremental network quantization: Towards lossless cnns with low-precision weights. *arXiv preprint arXiv:1702.03044*, 2017.
- Feng Zhu, Ruihao Gong, Fengwei Yu, Xianglong Liu, Yanfei Wang, Zhelong Li, Xiuqi Yang, and Junjie Yan. Towards unified int8 training for convolutional neural network. In *Proceedings of the IEEE/CVF Conference on Computer Vision and Pattern Recognition*, pages 1969–1979, 2020.
- Martin Zinkevich. Online convex programming and generalized infinitesimal gradient ascent. In *Proceedings of the 20th international conference on machine learning (icml-03)*, pages 928–936, 2003.

A Proof of Theorems

Lemma A.1 *If a function $\mathcal{L} : R^d \rightarrow R$ is convex, then for all $x, y \in R^d$,*

$$\mathcal{L}(y) \geq \mathcal{L}(x) + \nabla \mathcal{L}(x)^T (y - x).$$

Lemma A.2 *Let $\hat{\nabla}_{\Theta_t} = \hat{\nabla} \mathcal{L}_t(\Theta_t)$ and $\hat{\nabla}_{\Theta_{1:t}}$ be defined as above and bounded, $\|\hat{\nabla}_{\Theta_t}\|_2 \leq G$, $\|\hat{\nabla}_{\Theta_t}\|_\infty \leq G_\infty$. Then,*

$$\sum_{t=1}^T \sqrt{\frac{\hat{\nabla}_{\Theta_{t,i}}^2}{t}} \leq 2G_\infty \|\hat{\nabla}_{\Theta_{1:T,i}}\|_2.$$

Lemma A.3 *Let $\gamma \triangleq \frac{\beta_1^2}{\sqrt{\beta_2}}$. For $\beta_1, \beta_2 \in [0, 1)$ that satisfy $\frac{\beta_1^2}{\sqrt{\beta_2}} < 1$ and bounded $\hat{\nabla}_{\Theta_t}$, $\|\hat{\nabla}_{\Theta_t}\|_2 \leq G$, $\|\hat{\nabla}_{\Theta_t}\|_\infty \leq G_\infty$, the following inequality holds*

$$\sum_{t=1}^T \frac{\hat{m}_{t,i}^2}{\sqrt{t\hat{v}_{t,i}}} \leq \frac{2}{1-\gamma} \frac{1}{\sqrt{1-\beta_2}} \|\hat{\nabla}_{\Theta_{1:T,i}}\|_2.$$

The above lemma has been previously proven in Kingma and Ba [2014], and we omit its reproof here for brevity.

Lemma A.4 *For a random matrix \mathbf{X} , the following inequality holds*

$$\mathbb{E}[\|\mathbf{X}\|_2] \leq \sqrt{\mathbb{E}[\|\mathbf{X}\|_2^2]}$$

Proof. According to the formula $\mathbb{E}[x^2] = \text{Var}[x] + \mathbb{E}^2[x]$, we can derive:

$$\begin{aligned} \sqrt{\mathbb{E}[\|\mathbf{X}\|_2^2]} &= \sqrt{\mathbb{E}^2[\|\mathbf{X}\|_2] + \text{Var}[\|\mathbf{X}\|_2]} \\ &\geq \sqrt{\mathbb{E}^2[\|\mathbf{X}\|_2]} \\ &= \mathbb{E}[\|\mathbf{X}\|_2]. \end{aligned}$$

A.1 Theorem 4.3: Convergence of SGD

Proof. The iteration form of SGD is

$$\Theta_{t+1} \leftarrow \Theta_t - \alpha_t \hat{\nabla}_{\Theta_t}.$$

Subtract the scalar Θ^* and square both sides of the above update, we have,

$$\|\Theta_{t+1} - \Theta^*\|^2 - \|\Theta_t - \Theta^*\|^2 = -2\alpha_t \hat{\nabla}_{\Theta_t}(\Theta_t - \Theta^*) + \alpha_t^2 \hat{\nabla}_{\Theta_t}^2.$$

Taking exception on both sides and use Assumption 4.1, 4.2 and Lemma A.1, we have

$$\begin{aligned} \|\Theta_{t+1} - \Theta^*\|^2 - \|\Theta_t - \Theta^*\|^2 &= -2\alpha_t \nabla_{\Theta_t}(\Theta_t - \Theta^*) + \alpha_t^2 \mathbb{E}[\hat{\nabla}_{\Theta_t}^2] \\ &\leq -2\alpha_t [\mathcal{L}_t(\Theta_t) - \mathcal{L}_t(\Theta^*)] + \alpha_t^2 \sum_{i=1}^d (\mathbb{E}[\hat{\nabla}_{\Theta_{t,i}}^2]) \\ &\leq -2\alpha_t [\mathcal{L}_t(\Theta_t) - \mathcal{L}_t(\Theta^*)] + \alpha_t^2 d(\sigma^2 + e^2). \end{aligned}$$

Using $\alpha \geq \alpha_t$, we have

$$\|\Theta_{t+1} - \Theta^*\|^2 - \|\Theta_t - \Theta^*\|^2 \leq -2\alpha [\mathcal{L}_t(\Theta_t) - \mathcal{L}_t(\Theta^*)] + \alpha^2 d(\sigma^2 + e^2)$$

Sum up for $t = 1, \dots, T$,

$$\|\Theta_{T+1} - \Theta^*\|^2 - \|\Theta_1 - \Theta^*\|^2 \leq -2\alpha R^{SGD}(T) + \alpha^2 T d(\sigma^2 + e^2).$$

We can rearrange the above equation and $\|\Theta_n - \Theta_m\|_2 \leq D$,

$$\begin{aligned} R^{SGD}(T) &\leq \frac{\|\Theta_1 - \Theta^*\|^2 - \|\Theta_{T+1} - \Theta^*\|^2}{2\alpha} + \frac{\alpha T d(\sigma^2 + e^2)}{2} \\ &\leq \frac{D^2}{2\alpha} + \frac{\alpha T d(\sigma^2 + e^2)}{2} \end{aligned}$$

A.2 Theorem 4.5: Convergence of Adam

Proof. The iteration of Adam is

$$\begin{cases} m_t = \beta_{1,t} \cdot m_{t-1} + (1 - \beta_{1,t}) \cdot \hat{\nabla}_{\Theta_t}, \\ v_t = \beta_2 \cdot v_{t-1} + (1 - \beta_2) \cdot \left(\hat{\nabla}_{\Theta_t} \right)^2, \\ \hat{m}_t = \frac{m_t}{1 - \beta_1^t}, \hat{v}_t = \frac{v_t}{1 - \beta_2^t} \\ \Theta_{t+1} = \Theta_t - \frac{\alpha}{\sqrt{\hat{v}_t + \epsilon}} \cdot \hat{m}_t. \end{cases}$$

Using Lemma A.1, we have,

$$\mathcal{L}_t(\Theta_t) - \mathcal{L}_t(\Theta^*) \leq \nabla_{\Theta_t}^T (\theta_t - \theta^*) = \sum_{i=1}^d \nabla_{\Theta_{t,i}} (\Theta_{t,i} - \Theta_{*,i}^*).$$

From the above update rules presented, we have

$$\begin{aligned} \Theta_{t+1} &= \Theta_t - \alpha_t \hat{m}_t / \sqrt{\hat{v}_t} \\ &= \Theta_t - \frac{\alpha_t}{1 - \beta_1^t} \left(\frac{\beta_{1,t}}{\sqrt{\hat{v}_t}} m_{t-1} + \frac{(1 - \beta_{1,t})}{\sqrt{\hat{v}_t}} \hat{\nabla}_{\Theta_t} \right). \end{aligned}$$

For the i^{th} dimension of the parameter, we subtract the scalar $\Theta_{*,i}^*$ and square both sides of the above update rule, we have,

$$\begin{aligned} (\Theta_{t+1,i} - \Theta_{*,i}^*)^2 &= (\Theta_{t,i} - \Theta_{*,i}^*)^2 - \frac{2\alpha_t}{1 - \beta_1^t} \left(\frac{\beta_{1,t}}{\sqrt{\hat{v}_{t,i}}} m_{t-1,i} + \frac{(1 - \beta_{1,t})}{\sqrt{\hat{v}_{t,i}}} \hat{\nabla}_{\Theta_{t,i}} \right) (\Theta_{t,i} - \Theta_{*,i}^*) \\ &\quad + \alpha_t^2 \left(\frac{\hat{m}_{t,i}}{\sqrt{\hat{v}_{t,i}}} \right)^2. \end{aligned}$$

We can rearrange the above equation and use Young's inequality, $ab \leq a^2/2 + b^2/2$. Also, it can be shown that

$$\sqrt{\hat{v}_{t,i}} = \sqrt{\sum_{j=1}^t (1 - \beta_2) \beta_2^{t-j} \hat{\nabla}_{\Theta_{j,i}}^2 / \sqrt{1 - \beta_2^t}} \leq \|\hat{\nabla}_{\Theta_{1:t,i}}\|_2, \quad (5)$$

and $\beta_{1,t} \leq \beta_1$. Then

$$\begin{aligned} \hat{\nabla}_{\Theta_{t,i}} (\Theta_{t,i} - \Theta_{*,i}^*) &= \frac{(1 - \beta_1^t) \sqrt{\hat{v}_{t,i}}}{2\alpha_t (1 - \beta_{1,t})} \left((\Theta_{t,i} - \Theta_{*,i}^*)^2 - (\Theta_{t+1,i} - \Theta_{*,i}^*)^2 \right) \\ &\quad + \frac{\beta_{1,t}}{(1 - \beta_{1,t})} \frac{\hat{v}_{t-1,i}^{\frac{1}{4}}}{\sqrt{\alpha_{t-1}}} (\Theta_{*,i}^* - \Theta_{t,i}) \sqrt{\alpha_{t-1}} \frac{m_{t-1,i}}{\hat{v}_{t-1,i}^{\frac{1}{4}}} \\ &\quad + \frac{\alpha_t (1 - \beta_1^t) \sqrt{\hat{v}_{t,i}}}{2(1 - \beta_{1,t})} \left(\frac{\hat{m}_{t,i}}{\sqrt{\hat{v}_{t,i}}} \right)^2 \\ &\leq \frac{1}{2\alpha_t (1 - \beta_1)} \left((\Theta_{t,i} - \Theta_{*,i}^*)^2 - (\Theta_{t+1,i} - \Theta_{*,i}^*)^2 \right) \sqrt{\hat{v}_{t,i}} \\ &\quad + \frac{\beta_{1,t}}{2\alpha_{t-1} (1 - \beta_{1,t})} (\Theta_{*,i}^* - \Theta_{t,i})^2 \sqrt{\hat{v}_{t-1,i}} \\ &\quad + \frac{\beta_1 \alpha_{t-1}}{2(1 - \beta_1)} \frac{m_{t-1,i}^2}{\sqrt{\hat{v}_{t-1,i}}} + \frac{\alpha_t}{2(1 - \beta_1)} \frac{\hat{m}_{t,i}^2}{\sqrt{\hat{v}_{t,i}}}. \end{aligned}$$

We apply Lemma A.3 to the above inequality and sum across all the dimensions for $i \in 1, \dots, d$ and the iterations for $t \in 1, \dots, T$:

$$\begin{aligned}
\sum_{i=1}^d \sum_{t=1}^T \hat{\nabla}_{\Theta_{t,i}} (\Theta_{t,i} - \Theta_{*,i}^*) &\leq \sum_{i=1}^d \frac{1}{2\alpha(1-\beta_1)} (\Theta_{1,i} - \Theta_{*,i}^*)^2 \sqrt{\hat{v}_{1,i}} \\
&\quad + \sum_{i=1}^d \sum_{t=2}^T \frac{1}{2(1-\beta_1)} (\Theta_{t,i} - \Theta_{*,i}^*)^2 \left(\frac{\sqrt{\hat{v}_{t,i}}}{\alpha_t} - \frac{\sqrt{\hat{v}_{t-1,i}}}{\alpha_{t-1}} \right) \\
&\quad + \frac{\alpha(1+\beta_1)G_\infty}{(1-\beta_1)\sqrt{1-\beta_2}(1-\gamma)^2} \sum_{i=1}^d \|\hat{\nabla}_{\Theta_{1:T,i}}\|_2 \\
&\quad + \sum_{i=1}^d \sum_{t=1}^T \frac{\beta_{1,t}}{2\alpha_t(1-\beta_{1,t})} (\Theta_{*,i}^* - \Theta_{t,i})^2 \sqrt{\hat{v}_{t,i}}
\end{aligned}$$

From the assumption, $\|\Theta_t - \Theta^*\|_2 \leq D$, $\|\Theta_m - \Theta_n\|_\infty \leq D_\infty$, we have

$$\begin{aligned}
\sum_{i=1}^d \sum_{t=1}^T \hat{\nabla}_{\Theta_{t,i}} (\Theta_{t,i} - \Theta_{*,i}^*) &\leq \frac{D^2}{2\alpha(1-\beta_1)} \sum_{i=1}^d \sqrt{T\hat{v}_{T,i}} + \frac{D_\infty^2}{2\alpha} \sum_{i=1}^d \sum_{t=1}^T \frac{\beta_{1,t}}{(1-\beta_{1,t})} \sqrt{t\hat{v}_{t,i}} \\
&\quad + \frac{\alpha(1+\beta_1)G_\infty}{(1-\beta_1)\sqrt{1-\beta_2}(1-\gamma)^2} \sum_{i=1}^d \|\hat{\nabla}_{\Theta_{1:T,i}}\|_2
\end{aligned}$$

We apply Eq. 5 to the above inequality, we have

$$\begin{aligned}
\sum_{i=1}^d \sum_{t=1}^T \hat{\nabla}_{\Theta_{t,i}} (\Theta_{t,i} - \Theta_{*,i}^*) &\leq \frac{D^2\sqrt{T}}{2\alpha(1-\beta_1)} \sum_{i=1}^d \|\hat{\nabla}_{\Theta_{1:T,i}}\|_2 + \frac{D_\infty^2}{2\alpha} \sum_{i=1}^d \sum_{t=1}^T \frac{\beta_{1,t}\sqrt{t}}{(1-\beta_{1,t})} \|\hat{\nabla}_{\Theta_{1:t,i}}\|_2 \\
&\quad + \frac{\alpha(1+\beta_1)G_\infty}{(1-\beta_1)\sqrt{1-\beta_2}(1-\gamma)^2} \sum_{i=1}^d \|\hat{\nabla}_{\Theta_{1:T,i}}\|_2
\end{aligned}$$

Take expectation on both sides of the above inequality and apply Lemma A.4, Assumption 4.1,

$$\begin{aligned}
\sum_{i=1}^d \sum_{t=1}^T \nabla_{\Theta_{t,i}} (\Theta_{t,i} - \Theta_{*,i}^*) &\leq \frac{D^2\sqrt{T}}{2\alpha(1-\beta_1)} \sum_{i=1}^d \mathbb{E}[\|\hat{\nabla}_{\Theta_{1:T,i}}\|_2] \\
&\quad + \frac{\alpha(1+\beta_1)G_\infty}{(1-\beta_1)\sqrt{1-\beta_2}(1-\gamma)^2} \sum_{i=1}^d \mathbb{E}[\|\hat{\nabla}_{\Theta_{1:T,i}}\|_2] \\
&\quad + \frac{D_\infty^2}{2\alpha} \sum_{i=1}^d \sum_{t=1}^T \frac{\beta_{1,t}\sqrt{t}}{(1-\beta_{1,t})} \mathbb{E}[\|\hat{\nabla}_{\Theta_{1:t,i}}\|_2] \\
&\leq \frac{D^2\sqrt{T}}{2\alpha(1-\beta_1)} \sum_{i=1}^d \sqrt{\mathbb{E}[\|\hat{\nabla}_{\Theta_{1:T,i}}\|_2^2]} \\
&\quad + \frac{\alpha(1+\beta_1)G_\infty}{(1-\beta_1)\sqrt{1-\beta_2}(1-\gamma)^2} \sum_{i=1}^d \sqrt{\mathbb{E}[\|\hat{\nabla}_{\Theta_{1:T,i}}\|_2^2]} \\
&\quad + \frac{D_\infty^2}{2\alpha} \sum_{i=1}^d \sum_{t=1}^T \frac{\beta_{1,t}\sqrt{t}}{(1-\beta_{1,t})} \sqrt{\mathbb{E}[\|\hat{\nabla}_{\Theta_{1:t,i}}\|_2^2]} \\
&\leq \frac{D^2T}{2\alpha(1-\beta_1)} \sum_{i=1}^d \sqrt{\sigma^2 + e^2} + \frac{\alpha(1+\beta_1)G_\infty\sqrt{T}}{(1-\beta_1)\sqrt{1-\beta_2}(1-\gamma)^2} \sum_{i=1}^d \sqrt{\sigma^2 + e^2} \\
&\quad + \frac{D_\infty^2}{2\alpha} \sum_{i=1}^d \sum_{t=1}^T \frac{\beta_{1,t}t}{(1-\beta_{1,t})} \sqrt{\sigma^2 + e^2}.
\end{aligned}$$

We can use arithmetic geometric series upper bound for the last term:

$$\sum_{t=1}^T \frac{\beta_{1,t}}{(1-\beta_{1,t})} t \leq \sum_{t=1}^T \frac{1}{(1-\beta_1)} \lambda^{t-1} t \leq \frac{1}{(1-\beta_1)(1-\lambda)^2}$$

Therefore, we have the following regret bound:

$$\begin{aligned} R(T) &\leq \sum_{i=1}^d \sum_{t=1}^T \nabla_{\Theta_{t,i}} (\Theta_{t,i} - \Theta_{*,i}^*) \\ &\leq \frac{((1-\lambda)^2 D^2 T + D_\infty^2) d}{2\alpha(1-\beta_1)(1-\lambda)^2} \sqrt{\sigma^2 + e^2} + \frac{\alpha(1+\beta_1) G_\infty \sqrt{T} d}{(1-\beta_1) \sqrt{1-\beta_2(1-\gamma)^2}} \sqrt{\sigma^2 + e^2} \end{aligned}$$

B Variance of Specific Quantizers

Proposition B.1 (*Variance of stochastic rounding*) For any number $X \in \mathbb{R}$, $\text{Var}[\text{SR}(X)] \leq \frac{1}{4}$.

Proof. For any real number X , let $p := X - \lfloor X \rfloor \in [0, 1)$, then

$$\begin{aligned} \text{Var}[\text{SR}(X)] &= \mathbb{E}[\text{SR}(X) - X]^2 = p([\lfloor X \rfloor - X])^2 + (1-p)(\lfloor X \rfloor - X)^2 \\ &= p(1-p)^2 + p^2(1-p) = p(1-p)(1-p+p) = p(1-p) \leq \frac{1}{4}. \end{aligned}$$

B.1 Per-sample Quantizer

Given an activation gradient $\hat{\nabla}_{\mathbf{H}^{(l)}}$, its per-sample quantization is:

$$Q_g(\hat{\nabla}_{\mathbf{H}^{(l)}}) = \text{SR}(B(\hat{\nabla}_{\mathbf{H}^{(l)}} - \mathbf{Z}_i)/R_i)R_i/B + \mathbf{Z}_i,$$

where apply different ranges R_i and zero points Z_i for each sample of the gradient. When $\mathbf{S} = \text{diag}\{\frac{R_1}{B}, \dots, \frac{R_N}{B}\}$, we have

$$\begin{aligned} \text{Var}\left[Q_g\left(\hat{\nabla}_{\mathbf{H}^{(l)}}\right)\right] &= \text{Var}\left[\mathbf{S} \text{SR}\left(\left(\mathbf{S}^{-1}\left(\hat{\nabla}_{\mathbf{H}^{(l)}} - \mathbf{1Z}\right)\right) / + \mathbf{1Z}\right)\right] \\ &\leq \sum_{i=1}^N \sum_{j=1}^{D^{(l)}} \text{Var}\left[\frac{R_i}{B} \text{SR}\left(\frac{B}{R_i}\left(\hat{\nabla}_{\mathbf{H}^{(l)}} - \mathbf{Z}_i\right)\right) + \mathbf{Z}_i\right] \\ &= \sum_{i=1}^N \sum_{j=1}^{D^{(l)}} \frac{R_i^2}{B^2} \text{Var}\left[\text{SR}\left(\frac{B}{R_i}\left(\hat{\nabla}_{\mathbf{H}^{(l)}} - \mathbf{Z}_i\right)\right)\right] \\ &\leq \frac{D^{(l)}}{4B^2} \sum_{i=1}^N R_i^2. \end{aligned}$$

B.2 Per-sample Quantizer with AGP

Place the groups with the largest range in the first N/b rows, and let the range of these groups be denoted by $R_1, \dots, R_{N/b}$, groups in the remaining rows are denoted by $r_{N/b+1}, \dots, r_N$. We assume that $r/R \approx 0$.

$$Q_g(\hat{\nabla}_{\mathbf{H}^{(l)}}) = (\mathbf{MS}) \text{SR}\left(\left(\mathbf{MS}\right)^{-1}\left(\mathbf{M}\hat{\nabla}_{\mathbf{H}^{(l)}} - \mathbf{MZ}\right)\right) + \mathbf{MZ},$$

where $\mathbf{M} = \text{diag}\left(\frac{m_1}{p_1}, \dots, \frac{m_N}{p_N}\right)$, $p_i = \frac{NR_i}{bR_{\text{total}}}$, $R_{\text{total}} = \sum_{i=1}^N R_i$ and $m_i \sim \text{Bern}(p_i)$. To simplify the problem, we assume that $R_1 \approx R_2 \cdots \approx R_{N/b}$. And we use $r/R \approx 0$, then $p \approx \{1, \dots, 0\}$. In other words, for the first $\frac{N}{b}$ rows, $m = 1$, and 0 otherwise. We substitute it into the above equation and prune the groups with smaller ranges,

$$Q_g(\hat{\nabla}_{\mathbf{H}^{(l)}}) = \mathbf{S}_{1:\frac{N}{b}, 1:\frac{N}{b}} \text{SR}\left(\left(\mathbf{S}_{1:\frac{N}{b}, 1:\frac{N}{b}}\right)^{-1}\left(\hat{\nabla}_{\mathbf{H}^{(l)}} - \mathbf{1Z}_{1:\frac{N}{b}}\right)\right) + \mathbf{1Z}_{1:\frac{N}{b}}.$$

Then we have,

$$\begin{aligned}
\text{Var} \left[Q_g \left(\hat{\nabla}_{\mathbf{H}^{(l)}} \right) \right] &\leq \sum_{i=1}^{N/b} \sum_{j=1}^{D^{(l)}} \text{Var} \left[\frac{R_i}{B} \text{SR} \left(\frac{B}{R_i} (\hat{\nabla}_{\mathbf{H}^{(l)},i,j} - Z_i) \right) + Z_i \right] \\
&= \sum_{i=1}^{N/b} \sum_{j=1}^{D^{(l)}} \frac{R_i^2}{B^2} \text{Var} \left[\text{SR} \left(\frac{B}{R_i} (\hat{\nabla}_{\mathbf{H}^{(l)},i,j} - Z_i) \right) \right] \\
&\leq \frac{D^{(l)}}{4B^2} \sum_{i=1}^{N/b} R_i^2.
\end{aligned}$$

For 1-bit quantizers, the variance of PSQ is $\frac{D^{(l)}}{4} (\sum_{i=1}^{N/b} R_i^2 + \sum_{i=N/b+1}^N r_i^2)$. It is clear that

$$\frac{D^{(l)}}{4B^2} \sum_{i=1}^{N/b} R_i^2 \leq \frac{D^{(l)}}{4} \left(\sum_{i=1}^{N/b} R_i^2 + \sum_{i=N/b+1}^N r_i^2 \right).$$

C Implementation details

For simplicity, we use $\bar{\nabla}_{\mathbf{H}_{PSQ}^{(l)}}$ and $\bar{\nabla}_{\mathbf{H}_{PCQ}^{(l)}}$ to denote the low-bit versions quantized from $\mathbf{M}_{PSQ} \hat{\nabla}_{\mathbf{H}^{(l)}}$ and $\hat{\nabla}_{\mathbf{H}^{(l)}} \mathbf{M}_{PCQ}$. Extend this decomposition operation to the entire gradient tensor:

$$\begin{cases} \hat{\nabla}_{\mathbf{H}^{(l-1)}} = \sum_{i=1}^b 2^{(i-1)} (\mathbf{S}_{PSQ} (\bar{\nabla}_{\mathbf{H}_{PSQ}^{(l)}})^i \text{sign}(\Theta^{(l)\top})), \\ \hat{\nabla}_{\Theta^{(l)}} = \sum_{i=1}^b 2^{(i-1)} (\text{sign}(\mathbf{H}^{(l-1)\top}) (\bar{\nabla}_{\mathbf{H}_{PCQ}^{(l)}})^i \mathbf{S}_{PCQ}), \end{cases}$$

where both $(\bar{\nabla}_{\mathbf{H}_{PSQ}^{(l)}})^i$ and $(\bar{\nabla}_{\mathbf{H}_{PCQ}^{(l)}})^i$ represent the 1-bit tensors obtained after the decomposition. This transformation enables the implementation of most operations in backward propagation using XNOR and bit counting.

We implemented our method as a lightweight library in PyTorch. For binary matrix multiplication and some auxiliary operations, we implemented them using C++. In Alg. 1, we illustrate the process of forward and backward propagation for quantized fully connected layers. For simplicity, certain details, such as bias terms, quantization zero points, and the decomposition operations on gradient tensors, are omitted here. The entire process primarily consists of five components: quantization (9), encoding(4-5, 10), low-bit multiplication (6, 11), pruning (8), and dequantization (12).

Encoder is a functional component that encodes multiple integers with values of 1 or -1 into a smaller set of elements, facilitating subsequent XNOR operations. Taking Row_Encoder as an example, its primary form is illustrated in Alg. 2, the case where the number of columns is not divisible by b has been overlooked.

Binary multiplication is the crucial operation. In our approach, both forward and backward propagation are implemented through binary multiplication. For example, For two vectors, \mathbf{X}_1 and \mathbf{X}_2 , each of length 32, encode them into two unsigned 32-bit integers, x_1 and x_2 . The multiplication of the two is implemented as follows:

$$\text{SUM}(\mathbf{X}_1 \odot \mathbf{X}_2) = \text{bitcount}(\text{XNOR}(x_1, x_2)) \ll 1 - 32$$

where the dot product of two vectors, each of length 32, is efficiently replaced by a single bitcount and XNOR operation, effectively reducing energy consumption and time overhead. However, it is worth noting that an unbiased quantizer maps data to 0 or 1, rather than -1 or 1. Therefore, some conversion is required. For $\mathbf{X}_1 \in \{1, -1\}^n$, $\mathbf{X}_2 = \text{ReLU}(\mathbf{X}_1)$, it is clear that $(S/2)\mathbf{X}_1 + Z + (S/2) = S\mathbf{X}_2 + Z$. Therefore, some adjustments are needed: a straightforward modification of the scaling factor S and zero point Z is sufficient to achieve the transformation. This transformation requires only one multiplication and one addition for the scaling factor and zero point, thus incurring minimal overhead.

For convolutional layers, direct matrix multiplication is not feasible. To facilitate subsequent operations, an unfold is performed on the convolutional layer before matrix multiplication. After

Algorithm 1 Linear Layer Forward and Backward Propagation

- 1: **Input:** Input $\mathbf{H}^{(l-1)}$, Weight $\Theta^{(l)}$, Gradient of Loss $\nabla_{\mathbf{H}^{(l)}}$
 - 2: **Output:** Output $\mathbf{H}^{(l)}$, Gradient of Weight $\nabla_{\Theta^{(l)}}$, Gradient of Input $\nabla_{\mathbf{H}^{(l-1)}}$
 - 3: // Forward Propagation
 - 4: Encode Weight: $\tilde{\mathbf{H}}^{(l-1)} = \text{row_encoder}(\mathbf{H}^{(l-1)})$
 - 5: Encode Input: $\tilde{\Theta}^{(l)} = \text{column_encoder}(\Theta^{(l)})$
 - 6: Compute Output: $\mathbf{H}^{(l)} = \tilde{\mathbf{H}}^{(l-1)} \tilde{\Theta}^{(l)}$
 - 7: // Backward Propagation
 - 8: Pruning: $\nabla_{\mathbf{H}_{PSQ}^{(l)}}, \nabla_{\mathbf{H}_{PCQ}^{(l)}} = \text{pruner}(\nabla_{\mathbf{H}^{(l)}})$
 - 9: Quantization: $\bar{\nabla}_{\mathbf{H}_{PSQ}^{(l)}}, \mathbf{S}_{PSQ}^{(l)} = \text{PSQ}(\nabla_{\mathbf{H}_{PSQ}^{(l-1)}}),$
 $\bar{\nabla}_{\mathbf{H}_{PCQ}^{(l)}}, \mathbf{S}_{PCQ}^{(l)} = \text{PCQ}(\nabla_{\mathbf{H}_{PCQ}^{(l-1)}})$
 - 10: Encode Gradient: $\bar{\nabla}_{\mathbf{H}_{PSQ}^{(l)}} = \text{row_encoder}(\bar{\nabla}_{\mathbf{H}_{PSQ}^{(l)}}),$
 $\bar{\nabla}_{\mathbf{H}_{PCQ}^{(l)}} = \text{column_encoder}(\bar{\nabla}_{\mathbf{H}_{PCQ}^{(l)}})$
 - 11: Compute Gradient: $\bar{\nabla}_{\Theta^{(l)}} = \tilde{\mathbf{H}}^{(l-1)\top} \bar{\nabla}_{\mathbf{H}_{PCQ}^{(l)}},$
 $\bar{\nabla}_{\mathbf{H}^{(l-1)}} = \bar{\nabla}_{\mathbf{H}_{PSQ}^{(l)}} \tilde{\Theta}^{(l)\top}$
 - 12: Dequantization: $\hat{\nabla}_{\Theta^{(l)}} = \bar{\nabla}_{\Theta^{(l)}} \mathbf{S}_{PCQ}^{(l)}, \hat{\nabla}_{\mathbf{H}^{(l-1)}} = \mathbf{S}_{PSQ}^{(l)} \bar{\nabla}_{\mathbf{H}^{(l-1)}}$
 - 13: // Update Parameters
 - 14: Update Weight: $\mathbf{W} \leftarrow \mathbf{W} - \alpha \hat{\nabla}_{\Theta^{(l)}}$
-

Algorithm 2 Row_Encoder

- 1: **Input:** Input $\mathbf{H} \in \mathbb{R}^{N \times D}$, Bits b
 - 2: **Output:** Output $\mathbf{H}_e \in \mathbb{R}^{N \times \lfloor (1+(D-1)/b) \rfloor}$
 - 3: **for** $i \leftarrow 1$ to N **do**
 - 4: **for** $j \leftarrow 1$ to $\lfloor (1+(D-1)/b) \rfloor$ **do**
 - 5: $\mathbf{H}_{i,j} = 0$
 - 6: **for** $k \leftarrow 1$ to b **do**
 - 7: $s = (\mathbf{H} > 0)$
 - 8: $\mathbf{H}_{i,j} = (\mathbf{H}_{i,j} \ll k) \| s$
 - 9: **end for**
 - 10: **end for**
 - 11: **end for**
-

computation, the standard form is restored through folder operations. For example, We perform a convolution operation between the input $\mathbf{X} \in \mathbb{R}^{N \times C \times H \times W}$ and parameters $\Theta \in \mathbb{R}^{D \times C \times K \times K}$ to obtain the output $\mathbf{Y} \in \mathbb{R}^{N \times D \times H \times W}$.

1-bit Matrix Multiplication vs. Average 1-bit Matrix Multiplication. Given that our method is not a true 1-bit FQT but rather an average 1-bit FQT, we analyze the computational differences between the two approaches. In the case of $b=4$, the "average 1-bit matrix multiplication" first prunes a matrix to one-fourth of its original size. The remaining elements in this pruned matrix have a bit-width of 4 bits, ensuring an average bit-width of 1 bit. Subsequently, this pruned matrix is multiplied with another true 1-bit matrix. The computation process is as follows: based on the lossless decomposition described in the paper, the 4-bit matrix is decomposed into four equally sized 1-bit matrices. Subsequently, each of these four matrices undergoes true 1-bit matrix multiplication with the genuine 1-bit matrix. Finally, the four resulting matrices are merged together (Fig. 7). The operations involved in 1-bit matrix multiplication of the four submatrices are equivalent to those used in true 1-bit matrix multiplication, so no further analysis is required. For the decomposition operation, it can be accomplished through bitwise AND and shift operations. As for the final merging operation, it can be achieved using shift operations and integer addition. Moreover, the number of computations involved in both operations is at the level of the matrix size. In summary, while average 1-bit matrix multiplication requires additional decomposition and merging operations compared to

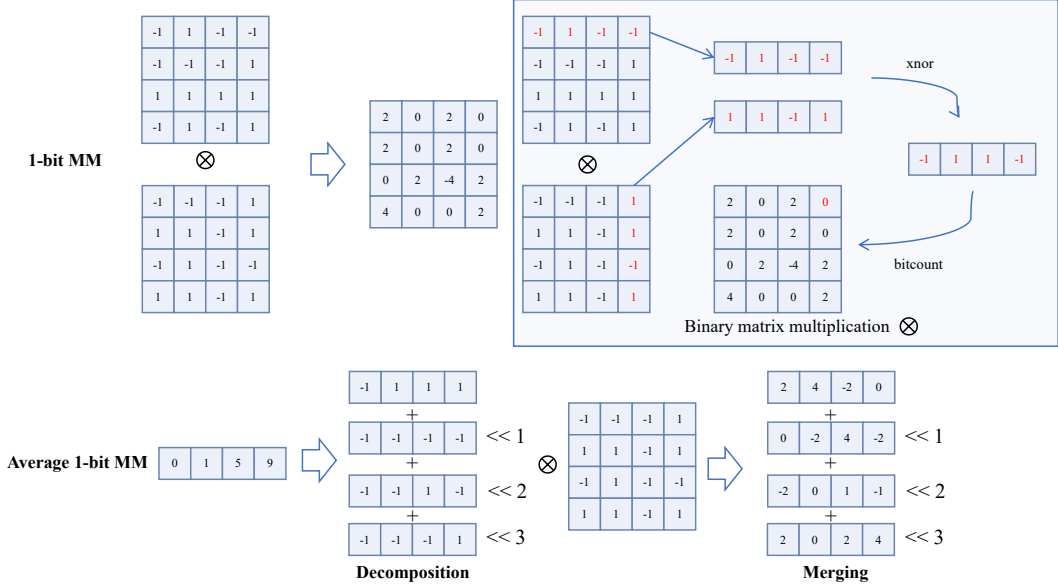


Figure 7: The calculation process of average 1-bit matrix multiplication and 1-bit matrix multiplication.

true 1-bit matrix multiplication, these operations can be achieved using bitwise AND, shift, and integer addition operations. The overhead associated with these operations is relatively low.

Unfolder treats each element involved in element-wise multiplication within the kernel as a row, and the number of times the window slides as columns, the unfolded input and parameters transform into $\mathbf{X}_u \in \mathbb{R}^{NHW \times CK^2}$, $\Theta_u \in \mathbb{R}^{D \times CK^2}$. Finally, we need to restore the output $\mathbf{Y}_u \in \mathbb{R}^{NHW \times D}$ to its standard state.

Folder is the inverse operation of Unfolder, designed to restore the gradients of both the input and parameters $\nabla_{\mathbf{X}_u} \in \mathbb{R}^{NHW \times CK^2}$, $\nabla_{\Theta_u} \in \mathbb{R}^{D \times CK^2}$ to their standard states.

D Experimental Details

D.1 Gradient distribution

From Fig. 8, it can be observed that the gradient of the activation exhibits a pattern across different epochs: the ranges of groups (both samples and dimensions) are highly uneven. Some groups have large ranges, while others have small ranges. Although we have presented results for a single batch, the same pattern persists across the remaining batches.

D.2 Experimental settings

Classification task: The training process is divided into two stages: initially undergoing quantization-aware training on ImageNet and subsequently undergoing FQT on various downstream datasets. The first stage: the initial learning rate was set to 10^{-3} and the weight decay to 10^{-5} , following Bulat and Tzimiropoulos [2019], the optimizer is Adam and use a cosine learning rate schedule. We train for 90 epochs. The second stage: for all datasets, the initial learning rate for fully connected layers is set to 10^{-3} . For portions of the network that have been previously trained, the learning rate is set to 10^{-5} , except for car dataset Krause et al. [2013] where it is set to 10^{-4} . The optimizer settings are the same as the first stage. We train for 60 epochs. The batch size was assigned to be 128. We measured training latency on CPUs, but to expedite the acquisition of accuracy statistics, we simulated the training results on 4 NVIDIA RTX A4000 GPUs. Due to limited resources on terminal devices, we utilized a smaller batch size of 64. We followed the configuration of Bulat and Tzimiropoulos

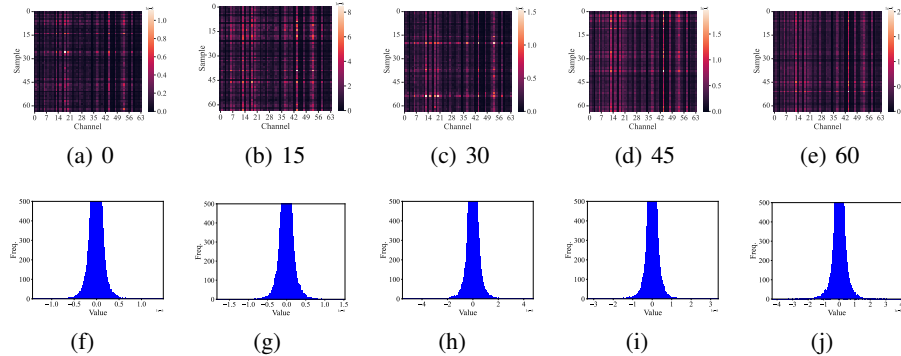


Figure 8: Heterogeneity in a ResNet18’s gradients. (a-e) Heatmap of the per-group range at the conv2.1.2 layer under different epochs; (f-j) Histogram of the gradient groups (samples) at the same layer.

Table 5: Experimental results on multiple downstream datasets. “(W, A, G)” denote the bitwidth of weight, activations, and gradients, respectively.

Method	Precision (W, A, G)	Accuracy(%)						
		CIFAR-10	CIFAR-100	Flowers	Cars	Pets	CUB	Average
Fine-tuning-Ours	1, 1, 1	78.03	57.47	79.71	38.27	71.19	39.64	60.72
Training-from-scratch-Ours	1, 1, 1	42.57	26.96	5.88	1.06	5.12	1.64	13.87
Training-from-scratch-PSQ	1, 1, 1	24.27	6.14	2.94	1.04	4.41	1.04	6.64

[2019] by excluding quantization for sensitive layers, such as the first and last layers, as well as skip connections in residual networks, in addition to batch normalization (BN) and ReLU layers.

Detection task: We evaluate our method on a simple transfer learning task to assess its effectiveness on object detection models, specifically transferring from high-resolution object detection to low-resolution object detection. The training process is divided into two stages: initially undergoing quantization-aware training on the PASCAL VOC 2007 and VOC 2012 trainval sets with a resolution of (600*600) pixels, followed by FQT training on the same dataset with a resolution of (300*300) pixels. The first stage: We followed all the settings of BiDet Wang et al. [2020], including the quantization methods for both weights and activation values and training configurations. The batch size was assigned to be 32, and the Adam optimizer was applied. The learning rate started from 10^{-3} and dropped during training every 6 epochs by a factor of 10. We train for 20 epochs. The second stage: the initial learning rate is 10^{-5} , the training epoch is 5 and the others are the same.

NLP tasks: We conduct experiments to validate the effectiveness of our proposed 1-bit FQT on BERT_{BASE} (12 hidden layers) and the GLUE benchmark Wang et al. [2018a] which consists of nine basic language tasks. We use the standard metrics for each GLUE task to evaluate our method. We use Spearman Correlation for STS-B, Mathews Correlation Coefficient for CoLA and classification accuracy for the rest tasks. As for MNLI task, we report the accuracy on both in-domain evaluation MNLI-match (MNLI-m) and cross-domain evaluation MNLI-mismatch (MNLI-mm). We exclude WNLI task as Qin et al. [2022]. We utilized BiBERT Qin et al. [2022] as our binarized model, which is derived by directly binarizing a full-precision one. Subsequently, we fine-tune this binarized model using both full-precision gradients (QAT) and 1-bit gradients (Ours). We follow Qin et al. [2022] by excluding quantization for classifier, position embedding layer, and token type embedding layer. We use the Adam as our optimizer. The training settings are also the same as Qin et al. [2022].

D.3 FQT from scratch

We compared the performance of our method in two scenarios: fine-tuning and training from scratch. We presented the classification results under the optimal configuration (b=4) in Table 5. From the table, it is evident that when training from scratch, the model exhibits very low classification accuracy across all datasets, and in certain datasets, it even lacks classification capability entirely. We attempted to analyze the differences between the two scenarios based on the distinct gradient

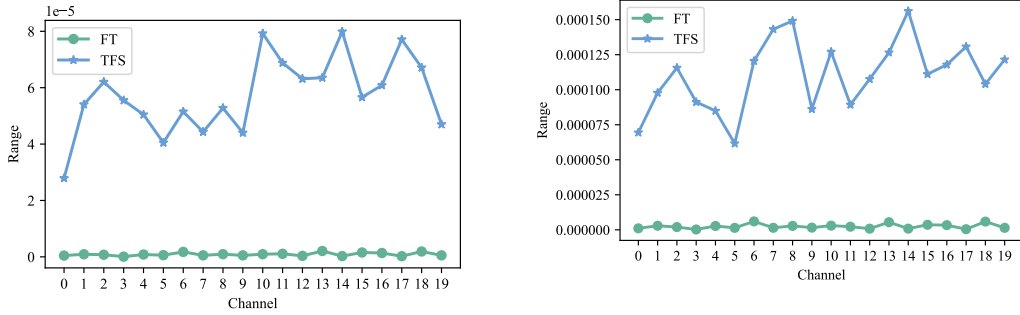


Figure 9: Gradient range analysis in ResNet18’s conv2.1.2 layer under fine-tuning (FT) and training from scratch (TFS). (left) The result from CIFAR-10. (right) The result from CIFAR-100.

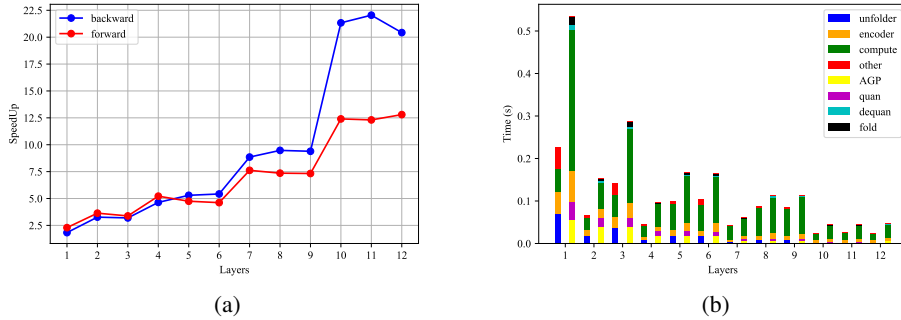


Figure 10: (a) The speedup of ours compared with FP32 PyTorch. (b) The compositional structure of time consumption.

distributions. From Fig. 9, we observe that the gradient range is larger in training from scratch, leading to increased gradient variance (Eq. 4) and reduced model convergence. Therefore, 1-bit FQT from scratch remains an open problem. Additionally, we also compared our method with PSQ in the scenario of training from scratch, and the results indicate that our approach still significantly outperforms PSQ in accuracy.

D.4 Time expenditure structure

We present the speedup across layers of VGGNet16 and the time consumption for each operation in Fig. 10, providing guidance for future optimization directions. It is important to note that the first and last layers were not quantized and, therefore, were not included in the analysis. From the figure, it is evident that matrix multiplication constitutes the majority of the training time, while the time overhead of other operations such as gradient pruning and quantization can be considered negligible. Therefore, the focus of future optimization efforts will remain on matrix multiplication. Furthermore, it can be observed that our implemented method is particularly friendly for layers with a large number of convolutional kernels and smaller input resolution.

NeurIPS Paper Checklist

1. Claims

Question: Do the main claims made in the abstract and introduction accurately reflect the paper's contributions and scope?

Answer: [Yes]

Justification: In Sec. 1, we state our contributions along with the scope and limitations of our method.

Guidelines:

- The answer NA means that the abstract and introduction do not include the claims made in the paper.
- The abstract and/or introduction should clearly state the claims made, including the contributions made in the paper and important assumptions and limitations. A No or NA answer to this question will not be perceived well by the reviewers.
- The claims made should match theoretical and experimental results, and reflect how much the results can be expected to generalize to other settings.
- It is fine to include aspirational goals as motivation as long as it is clear that these goals are not attained by the paper.

2. Limitations

Question: Does the paper discuss the limitations of the work performed by the authors?

Answer: [Yes]

Justification: In Sec. 1 and 7, we discuss the limitations of this study.

Guidelines:

- The answer NA means that the paper has no limitation while the answer No means that the paper has limitations, but those are not discussed in the paper.
- The authors are encouraged to create a separate "Limitations" section in their paper.
- The paper should point out any strong assumptions and how robust the results are to violations of these assumptions (e.g., independence assumptions, noiseless settings, model well-specification, asymptotic approximations only holding locally). The authors should reflect on how these assumptions might be violated in practice and what the implications would be.
- The authors should reflect on the scope of the claims made, e.g., if the approach was only tested on a few datasets or with a few runs. In general, empirical results often depend on implicit assumptions, which should be articulated.
- The authors should reflect on the factors that influence the performance of the approach. For example, a facial recognition algorithm may perform poorly when image resolution is low or images are taken in low lighting. Or a speech-to-text system might not be used reliably to provide closed captions for online lectures because it fails to handle technical jargon.
- The authors should discuss the computational efficiency of the proposed algorithms and how they scale with dataset size.
- If applicable, the authors should discuss possible limitations of their approach to address problems of privacy and fairness.
- While the authors might fear that complete honesty about limitations might be used by reviewers as grounds for rejection, a worse outcome might be that reviewers discover limitations that aren't acknowledged in the paper. The authors should use their best judgment and recognize that individual actions in favor of transparency play an important role in developing norms that preserve the integrity of the community. Reviewers will be specifically instructed to not penalize honesty concerning limitations.

3. Theory Assumptions and Proofs

Question: For each theoretical result, does the paper provide the full set of assumptions and a complete (and correct) proof?

Answer: [Yes]

Justification: In Sec. 4, theoretical results, including assumptions, are presented, with proofs provided in Appendix A.

Guidelines:

- The answer NA means that the paper does not include theoretical results.
- All the theorems, formulas, and proofs in the paper should be numbered and cross-referenced.
- All assumptions should be clearly stated or referenced in the statement of any theorems.
- The proofs can either appear in the main paper or the supplemental material, but if they appear in the supplemental material, the authors are encouraged to provide a short proof sketch to provide intuition.
- Inversely, any informal proof provided in the core of the paper should be complemented by formal proofs provided in appendix or supplemental material.
- Theorems and Lemmas that the proof relies upon should be properly referenced.

4. Experimental Result Reproducibility

Question: Does the paper fully disclose all the information needed to reproduce the main experimental results of the paper to the extent that it affects the main claims and/or conclusions of the paper (regardless of whether the code and data are provided or not)?

Answer: [Yes]

Justification: In the supplementary materials, we offer the code to accomplish this.

Guidelines:

- The answer NA means that the paper does not include experiments.
- If the paper includes experiments, a No answer to this question will not be perceived well by the reviewers: Making the paper reproducible is important, regardless of whether the code and data are provided or not.
- If the contribution is a dataset and/or model, the authors should describe the steps taken to make their results reproducible or verifiable.
- Depending on the contribution, reproducibility can be accomplished in various ways. For example, if the contribution is a novel architecture, describing the architecture fully might suffice, or if the contribution is a specific model and empirical evaluation, it may be necessary to either make it possible for others to replicate the model with the same dataset, or provide access to the model. In general, releasing code and data is often one good way to accomplish this, but reproducibility can also be provided via detailed instructions for how to replicate the results, access to a hosted model (e.g., in the case of a large language model), releasing of a model checkpoint, or other means that are appropriate to the research performed.
- While NeurIPS does not require releasing code, the conference does require all submissions to provide some reasonable avenue for reproducibility, which may depend on the nature of the contribution. For example
 - (a) If the contribution is primarily a new algorithm, the paper should make it clear how to reproduce that algorithm.
 - (b) If the contribution is primarily a new model architecture, the paper should describe the architecture clearly and fully.
 - (c) If the contribution is a new model (e.g., a large language model), then there should either be a way to access this model for reproducing the results or a way to reproduce the model (e.g., with an open-source dataset or instructions for how to construct the dataset).
 - (d) We recognize that reproducibility may be tricky in some cases, in which case authors are welcome to describe the particular way they provide for reproducibility. In the case of closed-source models, it may be that access to the model is limited in some way (e.g., to registered users), but it should be possible for other researchers to have some path to reproducing or verifying the results.

5. Open access to data and code

Question: Does the paper provide open access to the data and code, with sufficient instructions to faithfully reproduce the main experimental results, as described in supplemental material?

Answer: [Yes]

Justification: In the supplementary materials, we offer the code.

Guidelines:

- The answer NA means that paper does not include experiments requiring code.
- Please see the NeurIPS code and data submission guidelines (<https://nips.cc/public/guides/CodeSubmissionPolicy>) for more details.
- While we encourage the release of code and data, we understand that this might not be possible, so “No” is an acceptable answer. Papers cannot be rejected simply for not including code, unless this is central to the contribution (e.g., for a new open-source benchmark).
- The instructions should contain the exact command and environment needed to run to reproduce the results. See the NeurIPS code and data submission guidelines (<https://nips.cc/public/guides/CodeSubmissionPolicy>) for more details.
- The authors should provide instructions on data access and preparation, including how to access the raw data, preprocessed data, intermediate data, and generated data, etc.
- The authors should provide scripts to reproduce all experimental results for the new proposed method and baselines. If only a subset of experiments are reproducible, they should state which ones are omitted from the script and why.
- At submission time, to preserve anonymity, the authors should release anonymized versions (if applicable).
- Providing as much information as possible in supplemental material (appended to the paper) is recommended, but including URLs to data and code is permitted.

6. Experimental Setting/Details

Question: Does the paper specify all the training and test details (e.g., data splits, hyper-parameters, how they were chosen, type of optimizer, etc.) necessary to understand the results?

Answer: [Yes]

Justification: In Sec. 6, we outline the core experimental setup, with the complete setup detailed in Appendix D.

Guidelines:

- The answer NA means that the paper does not include experiments.
- The experimental setting should be presented in the core of the paper to a level of detail that is necessary to appreciate the results and make sense of them.
- The full details can be provided either with the code, in appendix, or as supplemental material.

7. Experiment Statistical Significance

Question: Does the paper report error bars suitably and correctly defined or other appropriate information about the statistical significance of the experiments?

Answer: [Yes]

Justification: We report the mean and stddev of 3 runs for main results (visual classification task).

Guidelines:

- The answer NA means that the paper does not include experiments.
- The authors should answer "Yes" if the results are accompanied by error bars, confidence intervals, or statistical significance tests, at least for the experiments that support the main claims of the paper.
- The factors of variability that the error bars are capturing should be clearly stated (for example, train/test split, initialization, random drawing of some parameter, or overall run with given experimental conditions).
- The method for calculating the error bars should be explained (closed form formula, call to a library function, bootstrap, etc.)
- The assumptions made should be given (e.g., Normally distributed errors).

- It should be clear whether the error bar is the standard deviation or the standard error of the mean.
- It is OK to report 1-sigma error bars, but one should state it. The authors should preferably report a 2-sigma error bar than state that they have a 96% CI, if the hypothesis of Normality of errors is not verified.
- For asymmetric distributions, the authors should be careful not to show in tables or figures symmetric error bars that would yield results that are out of range (e.g. negative error rates).
- If error bars are reported in tables or plots, The authors should explain in the text how they were calculated and reference the corresponding figures or tables in the text.

8. Experiments Compute Resources

Question: For each experiment, does the paper provide sufficient information on the computer resources (type of compute workers, memory, time of execution) needed to reproduce the experiments?

Answer: [Yes]

Justification: We describe the type and model of compute workers in Sec. 6 and report the time of execution.

Guidelines:

- The answer NA means that the paper does not include experiments.
- The paper should indicate the type of compute workers CPU or GPU, internal cluster, or cloud provider, including relevant memory and storage.
- The paper should provide the amount of compute required for each of the individual experimental runs as well as estimate the total compute.
- The paper should disclose whether the full research project required more compute than the experiments reported in the paper (e.g., preliminary or failed experiments that didn't make it into the paper).

9. Code Of Ethics

Question: Does the research conducted in the paper conform, in every respect, with the NeurIPS Code of Ethics [https://neurips.cc/public/EthicsGuidelines?](https://neurips.cc/public/EthicsGuidelines)

Answer: [Yes]

Justification: I confirm that the paper complies with ethical guidelines in every aspect.

Guidelines:

- The answer NA means that the authors have not reviewed the NeurIPS Code of Ethics.
- If the authors answer No, they should explain the special circumstances that require a deviation from the Code of Ethics.
- The authors should make sure to preserve anonymity (e.g., if there is a special consideration due to laws or regulations in their jurisdiction).

10. Broader Impacts

Question: Does the paper discuss both potential positive societal impacts and negative societal impacts of the work performed?

Answer: [Yes]

Justification: In the discussion following the conclusion, we explored the potential positive impacts of our method; since our approach aims to accelerate network training, no significant negative effects were observed.

Guidelines:

- The answer NA means that there is no societal impact of the work performed.
- If the authors answer NA or No, they should explain why their work has no societal impact or why the paper does not address societal impact.
- Examples of negative societal impacts include potential malicious or unintended uses (e.g., disinformation, generating fake profiles, surveillance), fairness considerations (e.g., deployment of technologies that could make decisions that unfairly impact specific groups), privacy considerations, and security considerations.

- The conference expects that many papers will be foundational research and not tied to particular applications, let alone deployments. However, if there is a direct path to any negative applications, the authors should point it out. For example, it is legitimate to point out that an improvement in the quality of generative models could be used to generate deepfakes for disinformation. On the other hand, it is not needed to point out that a generic algorithm for optimizing neural networks could enable people to train models that generate Deepfakes faster.
- The authors should consider possible harms that could arise when the technology is being used as intended and functioning correctly, harms that could arise when the technology is being used as intended but gives incorrect results, and harms following from (intentional or unintentional) misuse of the technology.
- If there are negative societal impacts, the authors could also discuss possible mitigation strategies (e.g., gated release of models, providing defenses in addition to attacks, mechanisms for monitoring misuse, mechanisms to monitor how a system learns from feedback over time, improving the efficiency and accessibility of ML).

11. Safeguards

Question: Does the paper describe safeguards that have been put in place for responsible release of data or models that have a high risk for misuse (e.g., pretrained language models, image generators, or scraped datasets)?

Answer: [NA]

Justification: Since this paper focuses on accelerating network training, it does not present these risks.

Guidelines:

- The answer NA means that the paper poses no such risks.
- Released models that have a high risk for misuse or dual-use should be released with necessary safeguards to allow for controlled use of the model, for example by requiring that users adhere to usage guidelines or restrictions to access the model or implementing safety filters.
- Datasets that have been scraped from the Internet could pose safety risks. The authors should describe how they avoided releasing unsafe images.
- We recognize that providing effective safeguards is challenging, and many papers do not require this, but we encourage authors to take this into account and make a best faith effort.

12. Licenses for existing assets

Question: Are the creators or original owners of assets (e.g., code, data, models), used in the paper, properly credited and are the license and terms of use explicitly mentioned and properly respected?

Answer: [Yes]

Justification: The assets used in this paper are credited and the license is respected.

Guidelines:

- The answer NA means that the paper does not use existing assets.
- The authors should cite the original paper that produced the code package or dataset.
- The authors should state which version of the asset is used and, if possible, include a URL.
- The name of the license (e.g., CC-BY 4.0) should be included for each asset.
- For scraped data from a particular source (e.g., website), the copyright and terms of service of that source should be provided.
- If assets are released, the license, copyright information, and terms of use in the package should be provided. For popular datasets, paperswithcode.com/datasets has curated licenses for some datasets. Their licensing guide can help determine the license of a dataset.
- For existing datasets that are re-packaged, both the original license and the license of the derived asset (if it has changed) should be provided.

- If this information is not available online, the authors are encouraged to reach out to the asset’s creators.

13. **New Assets**

Question: Are new assets introduced in the paper well documented and is the documentation provided alongside the assets?

Answer: [Yes]

Justification: New assets introduced in the paper are well documented.

Guidelines:

- The answer NA means that the paper does not release new assets.
- Researchers should communicate the details of the dataset/code/model as part of their submissions via structured templates. This includes details about training, license, limitations, etc.
- The paper should discuss whether and how consent was obtained from people whose asset is used.
- At submission time, remember to anonymize your assets (if applicable). You can either create an anonymized URL or include an anonymized zip file.

14. **Crowdsourcing and Research with Human Subjects**

Question: For crowdsourcing experiments and research with human subjects, does the paper include the full text of instructions given to participants and screenshots, if applicable, as well as details about compensation (if any)?

Answer: [NA]

Justification: The paper does not involve crowdsourcing or research with human subjects.

Guidelines:

- The answer NA means that the paper does not involve crowdsourcing nor research with human subjects.
- Including this information in the supplemental material is fine, but if the main contribution of the paper involves human subjects, then as much detail as possible should be included in the main paper.
- According to the NeurIPS Code of Ethics, workers involved in data collection, curation, or other labor should be paid at least the minimum wage in the country of the data collector.

15. **Institutional Review Board (IRB) Approvals or Equivalent for Research with Human Subjects**

Question: Does the paper describe potential risks incurred by study participants, whether such risks were disclosed to the subjects, and whether Institutional Review Board (IRB) approvals (or an equivalent approval/review based on the requirements of your country or institution) were obtained?

Answer: [NA]

Justification: The paper does not involve crowdsourcing nor research with human subject.

Guidelines:

- The answer NA means that the paper does not involve crowdsourcing nor research with human subjects.
- Depending on the country in which research is conducted, IRB approval (or equivalent) may be required for any human subjects research. If you obtained IRB approval, you should clearly state this in the paper.
- We recognize that the procedures for this may vary significantly between institutions and locations, and we expect authors to adhere to the NeurIPS Code of Ethics and the guidelines for their institution.
- For initial submissions, do not include any information that would break anonymity (if applicable), such as the institution conducting the review.